Nuclear and Particle Physics

W E Burcham
and
M Jobes

Harlow, England • London • New York • Boston • San Francisco • Toronto
Sydney • Tokyo • Singapore • Hong Kong • Seoul • Taipei • New Delhi
Cape Town • Madrid • Mexico City • Amsterdam • Munich • Paris • Milan

Pearson Education Limited
Edinburgh Gate
Harlow, Essex CM20 2JE, England

and Associated Companies throughout the world

Visit us on the World Wide Web at:
http://www.pearsoned.co.uk

First published 1995

British Library Cataloguing in Publication Data
A catalogue entry for this title is available from the British Library.

ISBN 0-582-45088-8

Library of Congress Cataloging-in-Publication data
A catalog entry for this title is available from the Library of Congress.

10 9 8 7 6
08 07 06 05 04

Set by 16UU in Times New Roman
Printed and bound by Antony Rowe Ltd, Eastbourne

9 Hadron spectroscopy

Introduction · Formation experiments · Phase space considerations · Production experiments

9.1 Introduction

In section 7.2 we gave a brief description of the particle 'directory' in which the hadrons were subdivided into 'stable' particles (table 7.2) and resonances (figure 7.2), the only distinction being that the latter can decay via the strong interactions with lifetimes of the order of 10^{-23} s while the former are either truly stable or decay via the weak or electromagnetic interactions, and therefore have much longer lifetimes. The discovery of a large number of resonant states and the determination of their quantum numbers such as spin, parity, isospin, strangeness etc. had a major influence on the search for an underlying symmetry scheme which would explain the hadron spectrum. In this chapter we outline the techniques used to identify the resonances and determine their quantum numbers.

Baryon resonances are readily excited in *formation* experiments in which mesons (π or K) interact with target nuclei at relatively low energies. The scattering cross-section is measured at a series of energies and if the total centre-of-mass energy sweeps through the mass of a resonance the cross-section will vary according to the Breit–Wigner formula (sections 6.3.2 and 9.2.3) and will in general show a peak with an energy width dependent on the lifetime of the resonant state. Quantum numbers such as baryon number, isospin and strangeness may be ascribed by application of the conservation laws appropriate to the strong interaction but spin and parity values require an analysis of the differential cross-section for the scattering (section 9.2).

Meson (and baryon) resonances can be observed in *production*

experiments. These are performed at a fixed incident energy, which is higher than in formation experiments, and the cross-section for the production of a particular multiparticle final state is given by Fermi's golden rule (section 5.2.3). Resonance production in a selected group of final state particles can be seen as an enhancement of the *effective mass* M of the selected group; the mass is given by the relativistic expression ($c = 1$)

$$M^2 = \left(\sum_i E_i\right)^2 - \left(\sum_i \boldsymbol{p}_i\right)^2 \tag{9.1}$$

where E_i and $\boldsymbol{p}_i$ are the total energy and (vector) momentum of the ith particle in the group. In principle, spin-parity values may be obtained by analysing the angular distribution of the particles in their rest system.

9.2 *Formation experiments*

9.2.1 *The partial wave formalism*

For simplicity we consider the scattering of spinless particles and neglect the Coulomb interaction. The more common case of scattering of a spin 0 particle by a spin $\frac{1}{2}$ particle (e.g. π–p scattering) is a little more complicated but follows a similar pattern.

The scattering of two particles (masses m_1 and m_2) is described by the Schrödinger equation

$$i\hbar \frac{\partial \psi}{\partial t}(\boldsymbol{r}, \boldsymbol{R}, t) = \left[-\frac{\hbar^2}{2M}\nabla_R^2 - \frac{\hbar^2}{2\mu}\nabla_r^2 + V(r)\right]\psi(\boldsymbol{r}, \boldsymbol{R}, t) \tag{9.2}$$

where the relative and centre-of-mass coordinates are defined by

$$\boldsymbol{r} = \boldsymbol{r}_1 - \boldsymbol{r}_2$$

$$M\boldsymbol{R} = m_1\boldsymbol{r}_1 + m_2\boldsymbol{r}_2 \qquad (M = m_1 + m_2)$$

and μ is the reduced mass. We have assumed that the potential is static and depends only on the relative coordinates of the interacting particles. The operators ∇_R^2 and ∇_r^2 imply differentiation with respect to centre-of-mass and relative coordinates respectively. Equation (9.2) can be separated in a straightforward manner to give

$$\psi(\boldsymbol{r}, \boldsymbol{R}, t) = u(\boldsymbol{r})v(\mathrm{R}) \exp\left[-\frac{i(E_r + E_R)t}{\hbar}\right] \tag{9.3a}$$

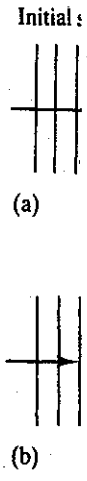

Figure 9
Schemat
the incic
in a scat
(a) an u
wave, u_i
approac
centre; (
consists
spherica
incident
$u_r \rightarrow$ exp

$$-\frac{\hbar^2}{2\mu}\nabla_r^2 u(\boldsymbol{r}) + V(r)u(\boldsymbol{r}) = E_r u(\boldsymbol{r}) \tag{9.3b}$$

$$-\frac{\hbar^2}{2M}\nabla_R^2 v(\boldsymbol{R}) = E_R v(\boldsymbol{R}) \tag{9.3c}$$

where E_r is the total energy in the centre-of-mass system and E_R is the energy associated with the motion of the centre of mass. Equation (9.3c) implies that the centre of mass of the two particles moves like a free particle with mass M and energy E_R. Equation (9.3b), which describes the relative motion of the two particles, has the same form as the equation which describes the scattering of a particle with reduced mass μ and energy E_r by a fixed scattering potential $V(r)$. It is this energy which is available for excitation or production of new particles and so equation (9.3b) forms our starting point for the partial wave formalism.

We assume that the potential $V(r)$ is of short range so that at large distances $V(r) \to 0$ and $u(r)$ satisfies the free particle wave equation

$$\nabla^2 u(\boldsymbol{r}) + k^2 u(\boldsymbol{r}) = 0 \tag{9.4}$$

with $k^2 = 2\mu E_r/\hbar^2$. Let us further assume that the incident particles are prepared in a state of definite momentum $\boldsymbol{p} = \hbar\boldsymbol{k}$ and that the beam propagates along the positive z axis. This initial state is then described by a plane wave

$$u_i = \exp(ikz) \tag{9.5}$$

as shown in figure 9.1(a). After the collision, in addition to the plane wave there must be an outgoing spherical wave originating at the scattering centre as shown in figure 9.1(b). The asymptotic form of the final state wavefunction may then be written as

$$u_f \to \exp(ikz) + \frac{\exp(ikr)}{r} f(\theta, \phi). \tag{9.6}$$

The second term in equation (9.6) corresponds to the outgoing spherical wave; it represents a particle moving radially outward from the scattering centre. The angles θ and ϕ are the usual polar and azimuthal angles of the momentum vector in a spherical polar coordinate system. The amplitude of the spherical wave can in principle depend on θ and ϕ; the dependence on r^{-1} ensures that the flux through a thin spherical shell at a distance r is independent of r.

A straightforward calculation of particle flux using the final state wavefunction u_f gives rise to interference terms between the incident plane wave and the outgoing spherical wave which are not present in practice.

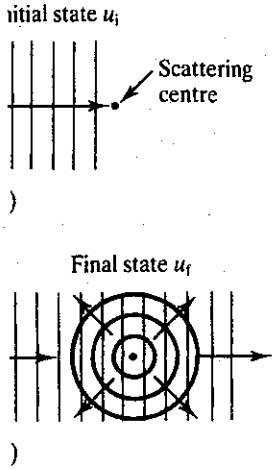

gure 9.1
hematic visualization of
e incident and final states
a scattering experiment:
) an unbounded plane
ve, $u_i = \exp(ikz)$,
proaches the scattering
ıtre; (b) the final state
nsists of an outgoing
herical wave and the
ident plane wave,
$\to \exp(ikz)$
$+ r^{-1}\exp(ikr)f(\theta, \phi)$.

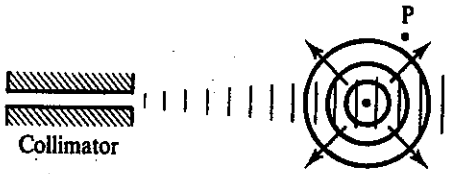

Figure 9.2 Schematic diagram showing the practical realization of a scattering experiment. The use of a collimator ensures that the incident beam is no longer unbounded as in figure 9.1 and the incident wave and scattered wave are effectively isolated. The contribution to the scattered intensity at the observation point P comes only from the outgoing spherical wave.

This is because in most experimental arrangements the incident and scattered particles are separated from each other by collimators. This difference between the theoretical situation, in which the incident plane wave is unbounded (figure 9.1), and a typical experimental situation is shown schematially in figure 9.2. In the practical case the incident beam is no longer infinite in extent but can be considered to be made up of a superposition of infinite plane waves whose propagation vectors differ slightly in magnitude and direction. Provided that the collimating apertures are not so small that diffraction effects become important, the angular spread of the incident beam is negligible; it is of the order of λ/d where λ is the wavelength associated with the incident particles and d is the width of the aperture. Since the function f in (9.6) varies only slowly with angle it is essentially unaffected by the small directional variation of the incident propagation vectors and in practice, if the scattered intensity is measured at the point of observation P, it is the spherical wave only that makes a contribution and this is virtually unchanged from that which appears in equation (9.6). Similarly, the incident flux (particles per unit area per unit time) arises from the plane wave term alone because at distances far enough from the scattering centre the second term in (9.6) becomes negligible.

The incident flux is obtained directly from the probability current density (example 9.3)

$$j(r, t) = \frac{\hbar}{2im}\left(\psi^*\nabla\psi - \psi\nabla\psi^*\right) \tag{9.7}$$

and substitution of the first term of (9.6) into (9.7) yields a flux v. For the scattered particles, substitution of the second term of (9.6) gives a flow of $v|f(\theta, \phi)|^2\,\mathrm{d}\Omega$ through an area subtending a solid angle $\mathrm{d}\Omega$ at the origin. From the definition of a differential cross-section (appendix B) it follows that

$$\frac{\mathrm{d}\sigma(\theta, \phi)}{\mathrm{d}\Omega} = \frac{\text{flow per unit time and solid angle}}{\text{incident flux}} = |f(\theta, \phi)|^2.$$

We note that, since the *scattered* wave is given by

$$u_{sc} = u_f - u_i = \frac{\exp(ikr)}{r} f(\theta, \phi) \tag{9.8}$$

the quantity $f(\theta, \phi)$ is known as the *scattering amplitude.*

It is apparent that in the description so far, even in the practical case of a collimated incident beam, the position of a particle with respect to the x and y axes cannot be specified completely and the angular momentum $l\hbar$ with respect to the scattering centre can have many values. It is therefore convenient to replace the plane wave by an equivalent series of spherical waves each of which represents a particle with a definite angular momentum about the scattering centre and with no component of angular momentum in the direction of incidence. Alternatively, since we are considering the scattering of a spinless particle by a central potential, there must be axial symmetry, which leads us to the expectation that the only spherical harmonics which can appear in the problem are those with no ϕ dependence, namely $Y_l^0(\theta)$.

The expansion of $\exp(ikz) = \exp(ikr\cos\theta)$ in spherical harmonics is[1]

$$\exp(ikz) = \sum_{l=0}^{\infty} \sqrt{[4\pi(2l+1)]}\, i^l j_l(kr)\, Y_l^0(\theta) \tag{9.9}$$

confirming that the incident wave decomposes into angular momentum states with $m = 0$ only. We require the asymptotic form of this expansion, for which we need the asymptotic behaviour of the spherical Bessel function

$$j_l(kr) \xrightarrow[kr \to \infty]{} \frac{1}{kr} \sin\left(kr - \frac{l\pi}{2}\right). \tag{9.10}$$

It is also convenient to write the spherical harmonic $Y_l^0(\theta)$ as

$$Y_l^0(\theta) = \left(\frac{2l+1}{4\pi}\right)^{1/2} P_l(\cos\theta) \tag{9.11}$$

where $P_l(\cos\theta)$ is a Legendre polynomial. Then

$$\exp(ikz) \to \frac{1}{kr} \sum_l (2l+1) i^l P_l(\cos\theta) \sin\left(kr - \frac{l\pi}{2}\right) \tag{9.12}$$

$$= \frac{1}{kr} \sum_l (2l+1) i^l P_l(\cos\theta) \times \frac{\exp[i(kr - l\pi/2)] - \exp[-i(kr - l\pi/2)]}{2i}. \tag{9.13}$$

Inspection of this last formula shows the plane wave can be considered as a series of spherical waves $\exp[-i(kr - l\pi/2)]$ each of definite angular momentum $l\hbar$ (partial waves) converging on the scattering centre together with a coherent superposition of diverging waves $\exp[i(kr - l\pi/2)]$. This situation represents an *undisturbed* incident plane wave. If now we consider an interaction with the scattering centre, causality requires that only the outgoing waves can be affected. The interaction potential may modify the outgoing waves in phase only or in amplitude and phase. In the former case we have *elastic scattering* with a certain angular distribution and in the latter case there are *inelastic processes* in addition. The steady state wavefunction when the interaction takes place may therefore be written

$$u_t = \frac{1}{kr}\sum_{l=0}^{\infty}(2l+1)i^l P_l(\cos\theta)a_l \times \frac{\exp[i(kr - l\pi/2)] - \exp[-i(kr - l\pi/2)]}{2i} \tag{9.14}$$

where a_l is a complex constant representing the effect of the scattering centre on the lth partial wave. The real part of a_l gives the change in amplitude and the imaginary part the change in phase. In accordance with equation (9.8) we can obtain an expression for the scattering amplitude, and hence the differential cross-section, by subtracting the incident wave u_i, in the form given by equation (9.13), from (9.14) and comparing coefficients of $\exp(ikr)$. The result is

$$f(\theta) = \frac{1}{2ik}\sum_{l=0}^{\infty}(2l+1)(a_l - 1)P_l(\cos\theta) \tag{9.15}$$

where use has been made of the identity $i^l = \exp[i(l\pi/2)]$. As expected, the scattering amplitude has no ϕ dependence. The differential cross-section is

$$\frac{d\sigma(\theta)}{d\Omega} = |f(\theta)|^2 = \frac{1}{k^2}\left|\sum_{l=0}^{\infty}(2l+1)\left(\frac{a_l - 1}{2i}\right)P_l(\cos\theta)\right|^2. \tag{9.16}$$

This expression refers to particles which are elastically scattered. The total cross-section for elastic scattering may be obtained by integration of (9.16);

$$\sigma_{el} = \int\frac{d\sigma(\theta)}{d\Omega}d\Omega = \int|f(\theta)|^2\,d\Omega = \frac{\pi}{k^2}\sum_{l=0}^{\infty}(2l+1)|1 - a_l|^2. \tag{9.17}$$

The last result follows from the orthonormality of the Legendre polynomials

$$\int P_l P_{l'} \, d\Omega = \frac{4\pi\delta_{ll'}}{2l+1} \tag{9.18}$$

where $\delta_{ll'}$ is the Kronecker δ symbol.

The change in amplitude and phase of the outgoing waves is commonly parametrized in terms of an inelasticity parameter η_l and a real phase shift δ_l. Then,

$$a_l = \eta_l \exp(2i\delta_l) \qquad \text{with } 0 \leqslant \eta_l \leqslant 1. \tag{9.19}$$

In the situation in which there is *elastic scattering* only, there must be no loss of incident particles and therefore $\eta_l = 1$. Substitution in equation (9.15) gives

$$f(\theta) = \frac{1}{k} \sum_{l=0}^{\infty} (2l+1) \frac{\exp(2i\delta_l) - 1}{2i} P_l(\cos\theta). \tag{9.20}$$

The association of δ_l with a phase shift becomes evident on substituting $a_l = \exp(2i\delta_l)$ in (9.14). The exponential term becomes

$$\frac{\exp[i(kr - l\pi/2 + 2\delta_l)] - \exp[-i(kr - l\pi/2)]}{2i}$$

so that $2\delta_l$ is the phase shift of the outgoing lth partial wave.

Again, substitution of $a_l = \exp(2i\delta_l)$ in (9.17) gives for the total elastic cross-section

$$\sigma_{el} = \frac{4\pi}{k^2} \sum_{l=0}^{\infty} (2l+1) \sin^2 \delta_l. \tag{9.21}$$

Since the scattering is elastic only, this also corresponds to the total scattering cross-section. It is apparent from (9.21) that the elastic cross-section associated with any particular l value or partial wave becomes a maximum if the phase shift δ_l passes through $\pi/2$; this condition is called a *resonance*. For a given partial wave, or angular momentum state, then, the maximum possible cross-section allowed by unitarity, or conservation of probability, is

$$\sigma_{el}^{max} = \frac{4\pi}{k^2}(2l+1) \qquad \sigma_{inel} = 0. \tag{9.22}$$

If the scattering centre is a *hard sphere* of radius R and if we consider the simple case of *low* incident energy ($kR \ll 1$) so that only $l = 0$ waves are involved then the corresponding phase shift may be obtained from equation (9.14) by imposing the requirement that the wave amplitude shall vanish on the surface of the sphere. This gives, with $\eta_l = 1$ for elastic scattering,

$$\exp(2i\delta_0) = \exp(-2ikR)$$

so that $\delta_0 = -kR$ and, from (9.21), taking $\sin \delta_0 \approx \delta_0$,

$$\sigma_{el} = 4\pi R^2.$$

This is the cross-section for the potential scattering referred to in section 6.3.2.

We turn now to the case in which the scattering process changes both the amplitude and the phase of the outgoing wave, i.e. there is some *inelastic* scattering. The inelastic cross-section is obtained by computing the *net* flow of particles associated with the wave u_t. This gives, using (9.14),

$$\sigma_{inel}^{max} = \frac{\pi}{k^2} \sum_{l=0}^{\infty} (2l + 1)(1 - |a_l|^2)$$

$$= \frac{\pi}{k^2} \sum_{l=0}^{\infty} (2l + 1)(1 - \eta_l^2). \tag{9.23}$$

The *total cross-section* is given by the sum of the elastic and inelastic cross-sections

$$\sigma_{tot} = \sigma_{el} + \sigma_{inel} = \frac{2\pi}{k^2} \sum_{l=0}^{\infty} (2l + 1)(1 - \mathrm{Re}\, a_l). \tag{9.24}$$

The maximum inelastic cross-section for a given partial wave is when $\eta_l = 0$ and then

$$\sigma_{inel}^{max} = \frac{\pi}{k^2}(2l + 1). \tag{9.25}$$

Notice that when the absorption or inelastic scattering has its maximum possible value there is still some elastic scattering with a maximum cross-section given by

$$\sigma_{el}^{max} = \sigma_{inel}^{max} = \frac{\pi}{k^2}(2l + 1). \tag{9.26}$$

It is thus possible to have elastic scattering without inelastic scattering, but if absorption takes place in a particular partial wave there must be some associated elastic scattering in the same partial wave: this is known as diffraction scattering.

Diffraction scattering is well marked in the classical or *high energy limit* ($kR \gg 1$) when the scatterer is completely absorbing for all partial waves up to the value $l = kR$ (*black disc*). Putting $a_l = 0$ for $0 \leqslant l \leqslant kR$ and $a_l = 1$ for $l > kR$ in (9.17) and (9.23) gives

$$\sigma_{\text{el}} = \sigma_{\text{inel}} = \frac{\pi}{k^2} \sum_0^{kR} (2l + 1) = \pi(R + \lambda\!\!\!^{-})^2$$

so that the total cross-section is $2\pi(R + \lambda\!\!\!^{-})^2 \approx 2\pi R^2$, in contrast with the classical expectation of πR^2. Physically it arises because of the need to create a 'shadow' behind the absorber; the diffraction scattering which thus arises has an angular distribution determined by the value of $1/kR = \lambda\!\!\!^{-}/R$.

9.2.2 *The optical theorem*

The total cross-section is related to the imaginary part of the forward scattering amplitude, a relationship known as the optical theorem. Previously we obtained for the scattering amplitude the expression

$$f(\theta) = \frac{1}{2ik} \sum_{l=0}^{\infty} (2l + 1)(a_l - 1) P_l(\cos\theta).$$

For forward scattering $\theta = 0$ and since $P_l(1) = 1$ we have

$$\begin{aligned} \text{Im } f(0) &= \text{Im}\left[\frac{1}{2k} \sum_{l=0}^{\infty} (2l + 1)\text{i}(1 - a_l)\right] \\ &= \frac{1}{2k} \sum_{l=0}^{\infty} (2l + 1)(1 - \text{Re } a_l). \end{aligned}$$

If we compare this expression with that for the total cross-section (9.24) we obtain the optical theorem:

$$\sigma_{\text{tot}} = \frac{4\pi}{k} \text{Im } f(0). \tag{9.27}$$

9.2.3 The partial wave amplitude and the Breit–Wigner formula

Let us define a partial wave amplitude

$$T_l(E) = \frac{\eta_l \exp(2i\delta_l) - 1}{2i} \tag{9.28}$$

and consider the behaviour of this amplitude as the energy E varies. For purely elastic scattering $\eta_l = 1$ and the partial wave amplitude may be written

$$T_l(E) = \exp(i\delta_l) \sin \delta_l = \frac{1}{\cot \delta_l - i}. \tag{9.29}$$

We have already seen in section 9.2.1 that the resonance condition is achieved as $\delta_l \to \pi/2$, so that near the resonant energy $\cot \delta_l \approx 0$. If E is the total energy of the colliding particles in the centre-of-mass system and E_R is the value of E at resonance, then in the neighbourhood of the resonance $\cot \delta_l$ can be expanded in a Taylor series to give

$$\cot[\delta_l(E)] = \cot[\delta_l(E_R)] + (E_R - E)\left\{\frac{d}{dE}\cot[\delta_l(E)]\right\}_{E=E_R} + \cdots. \tag{9.30}$$

At resonance $\cot[\delta_l(E_R)] = 0$ and if we define the quantity Γ through the relationship

$$\frac{2}{\Gamma} = \left\{\frac{d}{dE}\cot[\delta_l(E)]\right\}_{E=E_R} \tag{9.31}$$

then

$$T_l(E) = \frac{1}{(2/\Gamma)(E_R - E) - i} = \frac{\Gamma/2}{(E_R - E) - i\Gamma/2}. \tag{9.32}$$

For a given value of l the elastic partial wave cross-section (9.17) can be written

$$\sigma_{el}(E) = \frac{4\pi}{k^2}(2l + 1)|T_l(E)|^2 \tag{9.33}$$

and on substituting (9.32) into (9.33) we arrive at the celebrated Breit–Wigner resonance formula already used in section 6.3.2

$$\sigma_{el}(E) = \frac{4\pi}{k^2}(2l + 1)\frac{\Gamma^2/4}{(E_R - E)^2 + \Gamma^2/4}. \tag{9.34}$$

Equation (9.34) is specific to the case of spin-0–spin-0 scattering. The general case in which both the incident particle and the target particle have spin is treated in detail in reference 2. In this general case

$$\sigma_{el}(E) = \frac{4\pi}{k^2} g(J) \frac{\Gamma^2/4}{(E_R - E)^2 + \Gamma^2/4} \tag{9.35}$$

where the statistical weight for the channel spin J is

$$g(J) = \frac{2J + 1}{(2s_1 + 1)(2s_2 + 1)} \tag{9.36}$$

where s_1 and s_2 are the spins of the incident and target particles respectively.

Returning to the case of spin-0–spin-0 scattering, at an energy $E = E_R$ the elastic cross-section has its maximum value (equation (9.22))

$$\sigma_{el}^{max} = \frac{4\pi}{k^2}(2l + 1)$$

so that at any other energy

$$\frac{\sigma_{el}(E)}{\sigma_{el}^{max}} = \frac{\Gamma^2/4}{(E_R - E)^2 + \Gamma^2/4}. \tag{9.37}$$

At energies $E = E_R \pm \Gamma/2$ it is evident that $\sigma_{el}(E)/\sigma_{el}^{max} = \frac{1}{2}$ so that Γ is the full width at half maximum of the Breit–Wigner resonance shape. As pointed out already in chapter 7, the full width is related to the lifetime of the state through the uncertainty principle, $\Gamma\tau \approx \hbar$. For resonances decaying via the strong interactions the lifetimes are of the order of 10^{-23} s so that widths of 100 MeV or so are typical.

The above formulae are readily generalized to the case in which some inelastic scattering is present for which $\eta_l < 1$. The total width Γ of a resonance is the sum of the elastic (Γ_{el}) and inelastic (Γ_{in}) widths,

$$\Gamma = \Gamma_{el} + \Gamma_{in}$$

and the *elasticity* of a resonance is defined as

$$x = \frac{\Gamma_{el}}{\Gamma}.$$

The quantity

$$1 - x = \frac{\Gamma_{in}}{\Gamma}$$

is called the inelasticity. The probability of *formation* of the resonance in the elastic channel is proportional to x. The probability of *decay* into the elastic channel is also proportional to x while the probability of decay into any inelastic channel is proportional to $1 - x$. The elastic, inelastic and total cross-sections will therefore be proportional to x^2, $x(1-x)$ and x respectively, or equivalently to Γ_{el}^2, $\Gamma_{el}\Gamma_{in}$ and $\Gamma_{el}\Gamma$. In summary, the non-relativistic generalizations of the Breit–Wigner resonance formula are

$$\sigma_{el}(E) = \frac{\pi}{k^2} g(J) \frac{\Gamma_{el}^2}{(E_R - E)^2 + \Gamma^2/4} \tag{9.38}$$

$$\sigma_{in}(E) = \frac{\pi}{k^2} g(J) \frac{\Gamma_{el}\Gamma_{in}}{(E_R - E)^2 + \Gamma^2/4} \tag{9.39}$$

$$\sigma_{tot}(E) = \frac{\pi}{k^2} g(J) \frac{\Gamma_{el}\Gamma}{(E_R - E)^2 + \Gamma^2/4}. \tag{9.40}$$

Let us now consider the behaviour of the partial wave amplitude (9.28) in the vicinity of a resonance for both elastic and inelastic scattering. We use the symbol α to denote the elastic channel and β to denote an inelastic channel. Following convention, the amplitude is written as $T_{\alpha\alpha}$ for elastic scattering, e.g. $K^-p \to K^-p$, and as $T_{\alpha\beta}$ for inelastic scattering, e.g. $K^-p \to \Sigma^-\pi^+$. Then (9.28) becomes

$$T_{\alpha\alpha} = \frac{\eta_l \exp(2i\delta_l) - 1}{2i}.$$

The Breit–Wigner approximation for the elastic amplitude in the new notation becomes

$$T_{\alpha\alpha} = \frac{\Gamma_\alpha/2}{(E_R - E) - i\Gamma/2} = \frac{x_\alpha}{\epsilon - i} \tag{9.41}$$

where we have written the elastic width as Γ_α and the elasticity as $x_\alpha = \Gamma_\alpha/\Gamma$, where as before the total width is the sum of the partial widths

$$\Gamma = \sum_\gamma \Gamma_\gamma.$$

Furthermore, we have introduced the symbol $\epsilon = \cot \delta_l = 2(E_R - E)/\Gamma$. From (9.41) we note that

$$u = \mathrm{Re}\, T_{\alpha\alpha} = \frac{x_\alpha \epsilon}{\epsilon^2 + 1}$$

and

$$v = \text{Im } T_{\alpha\alpha} = \frac{x_\alpha}{\epsilon^2 + 1}.$$

When ϵ is eliminated from these equations it is found that

$$u^2 + \left(v - \frac{x_\alpha}{2}\right)^2 = \left(\frac{x_\alpha}{2}\right)^2$$

which is the equation of a circle with centre $(0, x_\alpha/2)$ and radius $x_\alpha/2$. When the only channel open is the elastic channel the scattering is perfectly elastic, $x_\alpha = 1$, and the radius of the circle is $\frac{1}{2}$, the so-called *unitarity* circle.

The Breit–Wigner approximation for the amplitude for the inelastic process leading from the channel α to the channel β is

$$T_{\alpha\beta} = \frac{\sqrt{(x_\alpha x_\beta)}}{\epsilon - \mathrm{i}}. \tag{9.42}$$

In this case the amplitude lies on a circle with centre $(0, \sqrt{(x_\alpha x_\beta)}/2)$ and radius $\sqrt{(x_\alpha x_\beta)}/2$.*

It is the aim of a partial wave analysis to determine, from the experimental differential cross-sections at different energies, the behaviour of the partial wave amplitudes as a function of energy and to look for resonant behaviour in particular partial waves. The results of a partial wave analysis are frequently presented in the form of an Argand diagram, i.e. a plot of Im T versus Re T as a function of the energy. For a resonant partial wave, $\epsilon = 0$ at the resonant energy $E = E_R$; the amplitude is purely imaginary and for a perfectly elastic resonance the representative point on the Argand diagram has coordinates (0, 1) as shown in figure 9.3(a). At energies $E < E_R$, ϵ is positive and for $E > E_R$ it is negative. The point (0, 0) on the Argand diagram corresponds to $\delta_l = 0, \pi \ldots$. If we assume that $\delta_l \to 0$ as $E \to 0$, or, in practice, for values of E well below the resonant energy, the representative point starts at (0, 0) and as the energy increases towards E_R moves around the unitarity circle in an *anticlockwise* direction. This property of the Breit–Wigner amplitude is a consequence of causality which restricts the amplitude to the form $(\cot \delta_l - \mathrm{i})^{-1}$ and excludes the complex conjugate amplitude, which

* Strictly, (9.42) should be written $T_{\alpha\beta} = \pm\sqrt{(x_\alpha x_\beta)}/(\epsilon - \mathrm{i})$, the sign being determined by the relative signs of the coupling of the elastic and inelastic channels to the resonant eigenstate, so that for an inelastic channel $T_{\alpha\beta}$ may be confined to the lower half-plane.

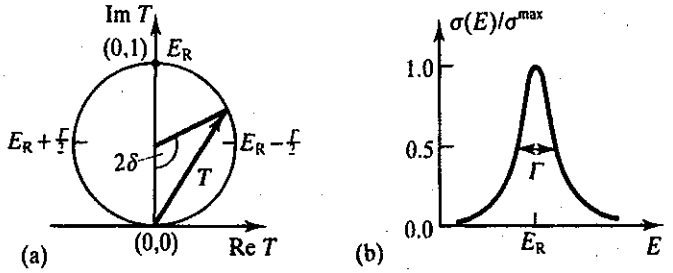

Figure 9.3 (a) An Argand diagram for a perfectly elastic resonance. When the imaginary part of the scattering amplitude T is plotted against the real part, the representative point moves around the unitarity circle in an anticlockwise direction as the energy increases. (b) The elastic cross-section showing the Breit–Wigner resonance shape.

would give the same cross-section but which would traverse the circle in a clockwise direction. This behaviour is known as the Wigner condition. Also shown in figure 9.3(b) is the corresponding behaviour of the elastic cross-section (9.37). The behaviour of the elastic amplitudes for isolated Breit–Wigner resonances with elasticities $x = 0.8$ and 0.4 are shown in figure 9.4. It should be noted that for $x > 0.5$ the phase shift passes through $\pi/2$ at resonance, as in the previous case discussed, but for $x < 0.5$ the phase shift passes through 0 at resonance.

In practice, a resonant partial wave amplitude does not always follow the idealized behaviour described above. In particular, if the amplitude contains a resonant contribution together with a non-resonant elastic background the characteristic circular motion of the amplitude in the Argand diagram may be shifted, rotated and distorted.

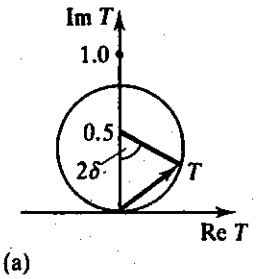

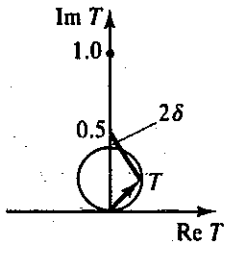

Figure 9.4
Argand diagrams for isolated Breit–Wigner resonances with elasticities (a) $x = 0.8$ and (b) $x = 0.4$.

9.2.4 *Some examples of baryon resonances*

At laboratory kinetic energies below 300 MeV, pion–nucleon scattering is dominated by the formation of the $\Delta(1232)$ resonance, the first resonant state to be discovered. The total cross-sections for π^+p and π^-p scattering are shown in figure 9.5. Large enhancements are seen in both cross-sections at an incident pion energy of 190 MeV, which corresponds to a total centre-of-mass energy of 1232 MeV or, equivalently, to a resonance mass of 1232 MeV/c^2. For pion–nucleon resonances the only possible values of the I spin are $\frac{1}{2}$ and $\frac{3}{2}$. Since the third component of I spin in the π^+p channel is $\frac{3}{2}$, the I spin of the $\Delta(1232)$ must be $\frac{3}{2}$. Confirmation of this assignment is given by the ratio (3:1) of the cross-sections in the π^+p and π^-p channels.

The spin of the $\Delta(1232)$ can be determined by application of the partial wave formalism developed in section 9.2.3.

However, in the present case of spin-0–spin-$\frac{1}{2}$ scattering each partial wave with a definite orbital angular momentum l has two values of J, namely $J = l \pm \frac{1}{2}$. During the collision there is some probability that the

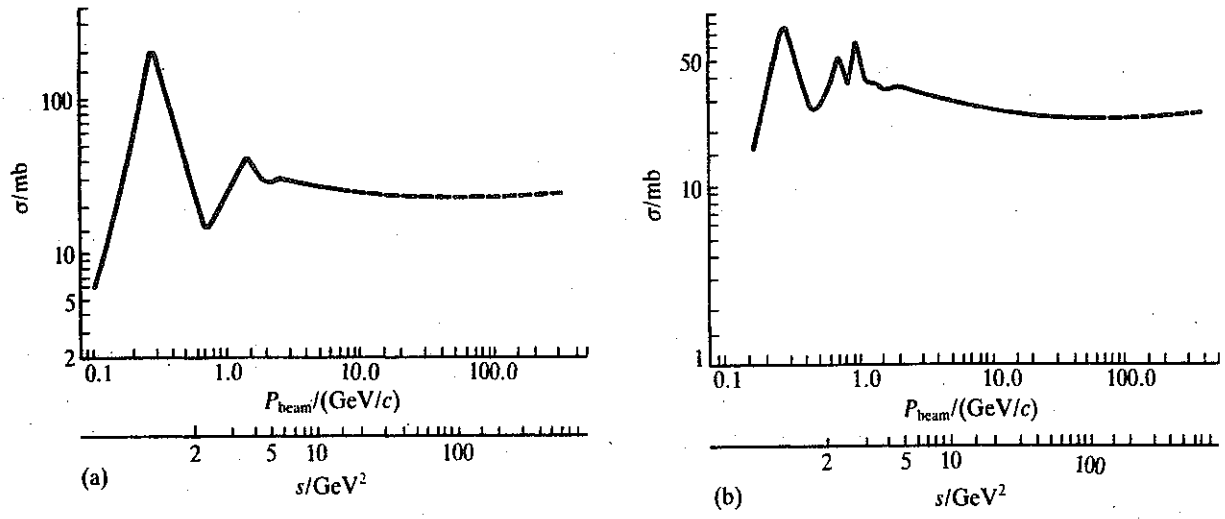

Figure 9.5 The total cross-sections for (a) π^+p and (b) π^-p scattering.

spin orientation may change but, since J_z must be conserved, any change in the z component of spin must be compensated by a corresponding change in the z component of the orbital angular momentum m. A 'spin-flip' interaction is therefore characterized by the appearance in the outgoing wave of a Legendre polynomial with non-zero m, i.e. an associated Legendre polynomial. The associated Legendre polynomials differ from the Legendre polynomials in their angular dependence and consequently the presence of spin affects the angular distribution of the scattered particles. Furthermore, since the spin-nonflip and spin-flip states are orthogonal, they will not interfere and the spin-flip states give rise to an *additional* contribution to the intensity of the scattered particles. Now, instead of the single amplitude, $f(\theta)$, there are two, a spin-nonflip amplitude

$$g(\theta) = \frac{1}{k}\sum_l [(l+1)T_{l+} + lT_{l-}]P_l^0(\cos\theta) \tag{9.43}$$

and a spin-flip amplitude

$$h(\theta) = \frac{1}{k}\sum_l (T_{l+} - T_{l-})P_l^1(\cos\theta). \tag{9.44}$$

T_{l+} and T_{l-}, the partial wave amplitudes for $J = l + \frac{1}{2}$ and $J = l - \frac{1}{2}$ respectively, have the same form as T_l in equation (9.28) and the differential cross-section now becomes

$$\frac{d\sigma}{d\Omega} = |g(\theta)|^2 + |h(\theta)|^2.$$

If we take the range of the π–N interaction as $R \approx 1/m_\pi$ then the values of orbital angular momentum which contribute to the scattering will be $l \approx kR = k/m_\pi$, so that for incident pion energies up to 300 MeV only S and P waves need to be considered. Then, equations (9.43) and (9.44) for the spin-nonflip and spin-flip amplitudes become

$$g(\theta) = \frac{1}{k}[T_{0,1/2} + (2T_{1,3/2} + T_{1,1/2})\cos\theta]$$

$$h(\theta) = \frac{1}{k}(T_{1,3/2} - T_{1,1/2})\sin\theta.$$

In these expressions the notation T_{IJ} has been used for the partial wave amplitudes and the explicit expressions for the Legendre polynomials, $P_0^0(\cos\theta) = 1$, $P_1^0(\cos\theta) = \cos\theta$ and $P_1^1(\cos\theta) = -\sin\theta$ have been inserted. The differential cross-section may then be written

$$\begin{aligned}\frac{d\sigma}{d\Omega} &= |g(\theta)|^2 + |h(\theta)|^2 \\ &= \frac{1}{k^2}(|T_{0,1/2} + (2T_{1,3/2} + T_{1,1/2})\cos\theta|^2 \\ &\quad + |T_{1,3/2} - T_{1,1/2}|^2 \sin^2\theta)\end{aligned} \tag{9.45}$$

which is of the form

$$\frac{d\sigma}{d\Omega} = \frac{1}{k^2}(A_0 + A_1\cos\theta + A_2\cos^2\theta) \tag{9.46}$$

with the identification

$$A_0 = |T_{0,1/2}|^2 + |T_{1,3/2} - T_{1,1/2}|^2 \tag{9.47a}$$

$$A_1 = 2\,\mathrm{Re}\,T^*_{0,1/2}(2T_{1,3/2} + T_{1,1/2}) \tag{9.47b}$$

$$A_2 = 3|T_{1,3/2}|^2 + 6\,\mathrm{Re}(T^*_{1,3/2}T_{1,1/2}). \tag{9.47c}$$

The expressions (9.47) show that the constant term in the differential cross-section has contributions from both S and P waves, the term in $\cos\theta$ is an interference term between the S and P waves while the quadratic term has a contribution from P waves only.

In essence, a partial wave analysis consists of determining the coefficients A_0, A_1 and A_2, or equivalently the partial wave amplitudes T_{IJ}, as a function of energy from the experimentally determined differential cross-sections. Figure 9.6 shows the differential cross-sections obtained by Bussey *et al.*[3] for π^+p elastic scattering as a function of energy. The

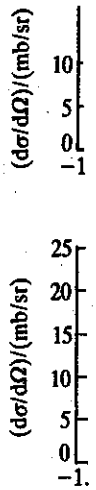

Figure 9.
1973 *Nuc*

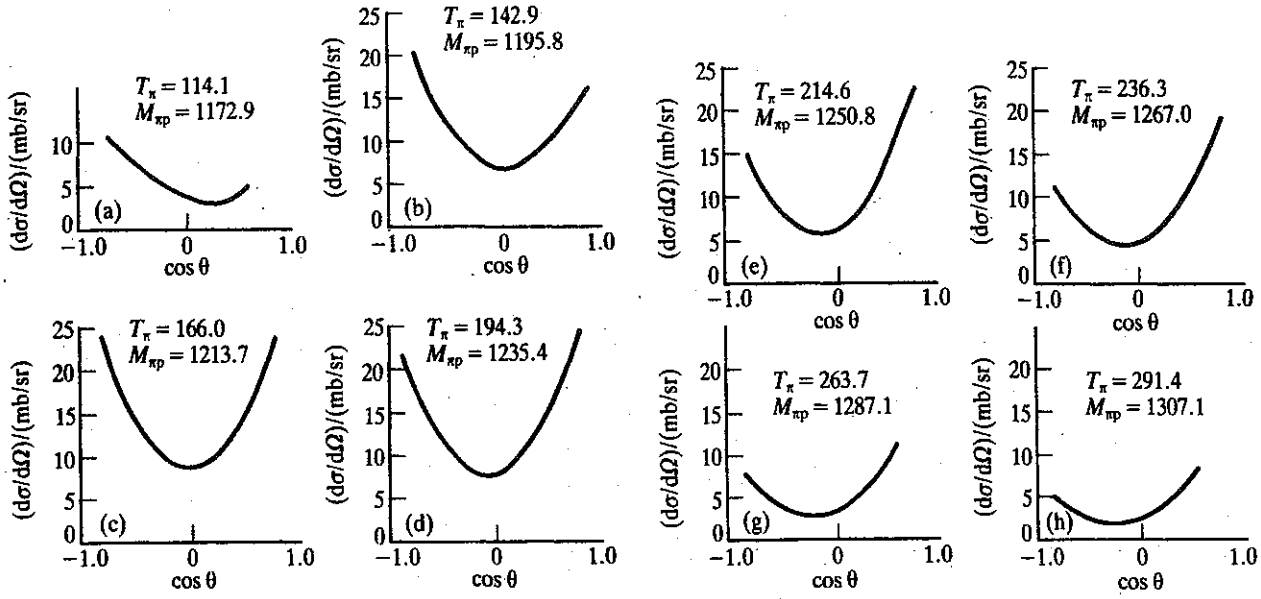

Figure 9.6 Differential cross-sections for π^+p elastic scattering at various incident pion energies. (After Bussey P J *et al.* 1973 *Nucl Phys* **B58** (363).)

asymmetry in the differential cross-section at the lowest energy shows that even at this energy the P wave amplitude is significant. As the energy sweeps through the resonant energy the distributions become symmetric about $\theta = \pi/2$ and above resonance interference is again evident. Figure 9.7(a) shows a typical variation of the coefficients A_0, A_1 and A_2 with energy. At resonance the values of these coefficients are very nearly 1, 0 and 3 respectively, i.e. the differential cross-section is

$$\frac{d\sigma}{d\Omega} = \frac{1}{k^2}(1 + 3\cos^2\theta). \tag{9.48}$$

This is precisely the form expected for the production in πp collisions of a $J^P = \frac{3}{2}^+$ state, which decays by pure P wave.

The notation $L_{2I,2J}$, where L is the orbital angular momentum, I is the I spin and J is the spin, is commonly used to describe π–N partial wave amplitudes. Figure 9.7(b) shows the Argand diagram for the P_{33} partial wave. It follows the unitarity circle, i.e. the P_{33} wave is perfectly elastic ($\eta = 1$). The phase shift passes through $\pi/2$ at the resonant energy 1232 MeV and at this energy the cross-section has its maximum value allowed by unitarity, i.e.

$$\sigma_{\max}^{el} = \frac{4\pi}{k^2}(J + \tfrac{1}{2}) = \frac{8\pi}{k^2}$$

for a $J = \frac{3}{2}$ resonance, as shown in figure 9.7(c).

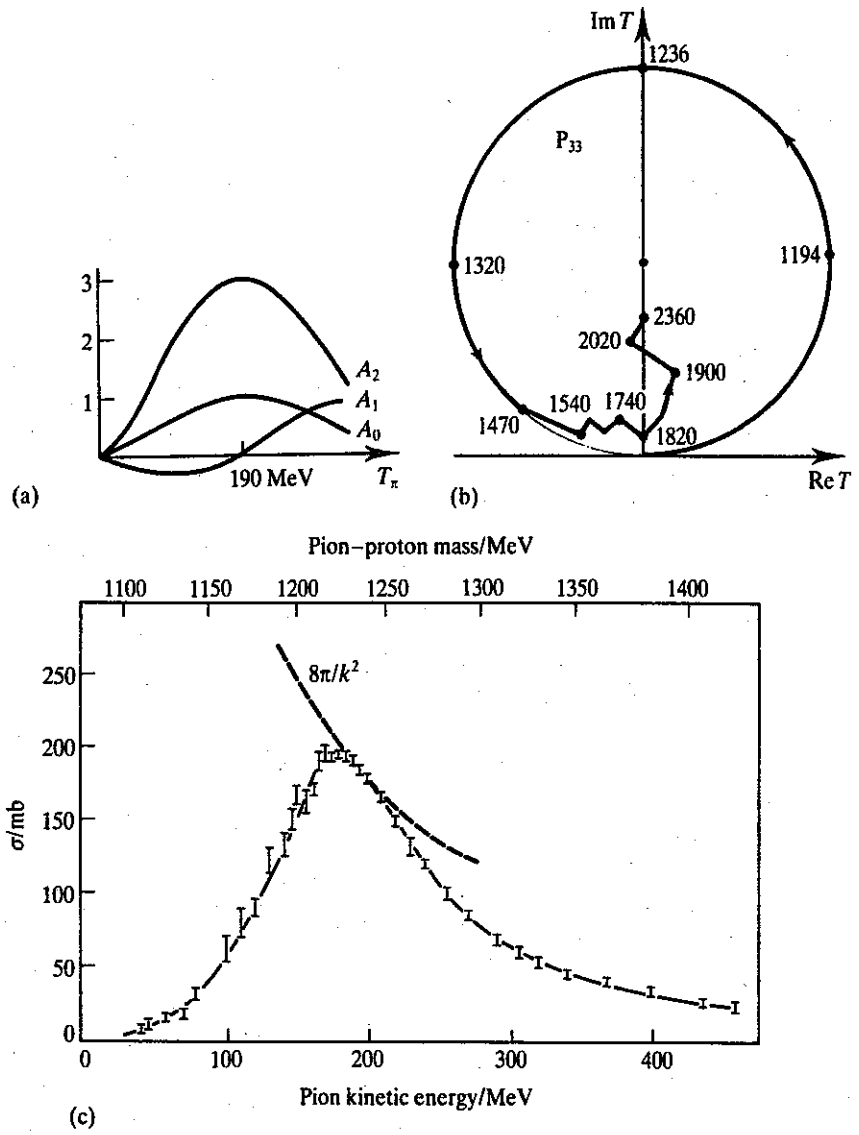

Figure 9.7 (a) Typical variation of the coefficients A_l in a fit of the differential cross-section to the formula $d\sigma/d\Omega = \Sigma A_n \cos^n \theta$; (b) Argand diagram for the perfectly elastic $\Delta(1232)$; (c) the total cross-section for $\pi^+ p$ scattering in the vicinity of the $\Delta(1232)$. The unitarity limit for a $J = \frac{3}{2}$ resonance $\sigma_{max} = 8\pi/k^2$ is also shown.

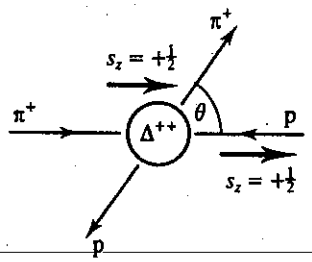

Figure 9.8
Formation and decay of the $\Delta^{++}(1232)$ viewed in the rest system of the resonance.

We now show that (9.48) is the expected angular distribution for the decay of a $J^P = \frac{3}{2}^+$ $\Delta(1232)$ produced in $\pi^+ p$ collisions. Let us take the direction of the incident π^+ in the centre-of-mass system as the quantization or z axis, and assume that the proton initially has its spin pointing in this direction. Since there can be no component of orbital angular momentum along the direction of incidence and because the z component of angular momentum must be conserved, the $\Delta^{++}(1232)$ must also have $s_z = +\frac{1}{2}$, i.e. the Δ^{++} is produced in the angular momentum state $|\frac{3}{2}, \frac{1}{2}\rangle$ (figure 9.8). Total angular momentum can be conserved in the decay either

by P wave ($l = 1$) or D wave ($l = 2$) emission since the proton spin can couple to either of these to give a total angular momentum of $\frac{3}{2}$. Conservation of parity in the decay, however, rules out the possibility of D wave emission. For P wave decay then, the spatial wavefunction of the final state πp system must contain spherical harmonics with $l = 1$. Since the z component of the total angular momentum in the final state must be $+\frac{1}{2}$, the overall wavefunction must be

$$\psi(\theta, \phi) = \sqrt{\tfrac{1}{3}}Y_1^1(\theta, \phi)|\tfrac{1}{2}, -\tfrac{1}{2}\rangle + \sqrt{\tfrac{2}{3}}Y_1^0(\theta, \phi)|\tfrac{1}{2}, \tfrac{1}{2}\rangle \tag{9.49}$$

where the coefficients $\sqrt{\frac{1}{3}}$ and $\sqrt{\frac{2}{3}}$ are the Clebsch–Gordan coefficients for the coupling of an angular momentum $l = 1$ and a spin $s = \frac{1}{2}$ (the proton spin) to the state $|J, J_z\rangle = |\frac{3}{2}, \frac{1}{2}\rangle$. Since

$$Y_1^0 = \sqrt{\left(\frac{3}{4\pi}\right)}\cos\theta \qquad \text{and} \qquad Y_1^1 = -\sqrt{\left(\frac{3}{8\pi}\right)}\sin\theta\, e^{i\phi}$$

the decay angular distribution is

$$\frac{d\sigma}{d\Omega} = |\psi(\theta, \phi)|^2 = \frac{1}{8\pi}(1 + 3\cos^2\theta). \tag{9.50}$$

In obtaining (9.50) from (9.49) we have made use of the orthonormality of the spin states $|\frac{1}{2}, \frac{1}{2}\rangle$ and $|\frac{1}{2}, -\frac{1}{2}\rangle$ so that in forming $|\psi(\theta, \phi)|^2$ the cross-terms disappear. Furthermore, explicit calculation, or parity conservation, shows that the same angular distribution results if the proton is initially in the state $|s, s_z\rangle = |\frac{1}{2}, -\frac{1}{2}\rangle$. Equation (9.50) has the same form as the differential cross-section (9.48).

As already indicated, a π^+p system can have $I = \frac{3}{2}$ only and consequently only $I = \frac{3}{2}$ resonances can be excited in π^+p formation experiments. In figure 9.5 structure in the π^+p total cross-section can be seen at centre-of-mass energies above the Δ(1232) resonance which suggests that there may be other, higher mass Δ resonances. This is indeed the case, but care must be taken in interpreting a bump in a total cross-section as a resonance. As the incident energy increases, more and more partial waves are brought into play and it is possible for non-resonant amplitudes to conspire to give structure in a total cross-section. Correspondingly, it is possible that in the presence of other non-resonant partial waves, a resonant partial wave may not be evident as a bump in a total cross-section. Many higher mass Δ resonances, i.e. resonances with baryon number $B = 1$, strangeness $S = 0$ and I spin $I = \frac{3}{2}$, have been identified in partial wave analyses,* although at energies above about 2 GeV the

* For detailed properties and full lists of references on these and all other particle states the reader is referred to the 'Review of particle properties' by the Particle Data Group.[4]

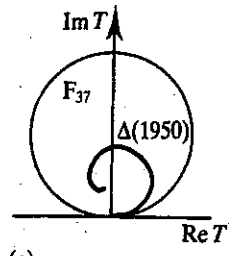

(a)

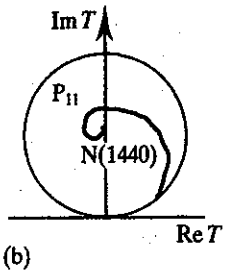

(b)

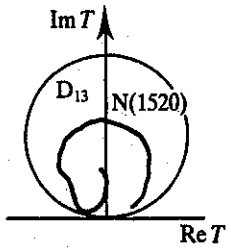

(c)

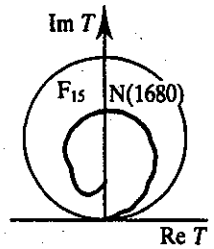

(d)

Figure 9.9
Argand diagrams for various inelastic πN resonances: (a) the F_{37} Δ(1950); (b) the P_{11} N(1440); (c) the D_{13} N(1520); (d) the F_{15} N(1680).

π^+p total cross-section is rather featureless. As an example the Argand diagram for the Δ(1950), a resonance in the F_{37} partial wave, is shown in figure 9.9(a). These partial wave analyses are similar in principle to that outlined above for low energy π^+p scattering but are in practice much more complicated because of the presence of many more partial waves.

A comparison of the total cross-section for π^-p scattering with that for π^+p scattering shows that in addition to the $\Delta^0(1232)$ there is structure in $\sigma_{tot}(\pi^-p)$ which is not present in $\sigma_{tot}(\pi^+p)$. This is because in the π^-p channel there are $I = \frac{1}{2}$ amplitudes in addition to the $I = \frac{3}{2}$ amplitudes. The decomposition of a π^-p system into I spin states $|I, I_3\rangle$ is

$$|\pi^-p\rangle = \sqrt{\tfrac{1}{3}}|\tfrac{3}{2}, -\tfrac{1}{2}\rangle - \sqrt{\tfrac{2}{3}}|\tfrac{1}{2}, -\tfrac{1}{2}\rangle \tag{9.51}$$

where, as usual, the factors $\sqrt{\frac{1}{3}}$ and $\sqrt{\frac{2}{3}}$ are Clebsch–Gordan coefficients. Thus, in terms of I spin the amplitude for elastic π^-p scattering may be written

$$\langle\pi^-p|T^I_{lJ}|\pi^-p\rangle = \langle\pi^-p|\tfrac{1}{3}T^{3/2}_{lJ} + \tfrac{2}{3}T^{1/2}_{lJ}|\pi^-p\rangle. \tag{9.52}$$

For each partial wave T_{lJ}, which is unique in the case of π^+p scattering but which strictly should have been written $T^{3/2}_{lJ}$, there are two partial wave amplitudes for each value of l and J in the case of π^-p scattering, one for each of the possible I spin values. Then, for low energy π^-p elastic scattering, with S and P waves only, the differential cross-section is obtained from that for π^+p scattering (equation (9.45)) by the replacement of the amplitudes T_{lJ} with $\frac{1}{3}(T^{3/2}_{lJ} + 2T^{1/2}_{lJ})$. The additional structure in $\sigma_{tot}(\pi^-p)$ can then be interpreted as due to the formation of resonances with $I = \frac{1}{2}$, which, since in addition have $B = 1$, $S = 0$ like the nucleon, are labelled N, with the mass of the resonance inserted, as usual, in brackets. As in the case of the $I = \frac{3}{2}$ Δ resonances, many $I = \frac{1}{2}$ nucleon resonances have been identified in phase shift analyses. As examples, we show in figures 9.9(b)–9.9(d) the Argand diagrams for the well-established P_{11} N(1440), the D_{13} N(1520) and the F_{15} N(1680) elastic amplitudes. Unlike the P_{33} Δ(1232) amplitude which, as we have seen, is perfectly elastic and follows the unitarity circle, these amplitudes are inelastic ($\eta < 1$) and lie well inside the unitarity circle. Because of the higher centre-of-mass energies involved in the formation of these resonances, various inelastic channels such as Δπ and Nρ are open. Then, in addition to the possibility of formation *and* decay via the elastic channel, decay to the final states Δπ and Nρ is also possible.

In this section we have illustrated the partial wave formalism through its application to low energy πN scattering. The technique is readily extended to other channels and in particular $\bar{K}$N formation experiments have proved fruitful in the determination of the quantum numbers of baryon resonances with non-zero strangeness. In this case the initial state has conserved quantum numbers $B = 1$ and $S = -1$ and, since the

interacting particles can couple to give either $I = 0$ or $I = 1$, both Λ ($I = 0$) and Σ ($I = 1$) resonances are produced. The KN channel is not so fruitful; the quantum numbers in the initial state are $B = 1$ and $S = +1$ and strangeness $+1$ baryons do not exist.

9.3 *Phase space considerations*

Fermi's golden rule states that the probability per unit time that a transition will take place from an initial state $|i\rangle$ to a final state $|f\rangle$ is

$$W = \frac{2\pi}{\hbar} |M_{fi}|^2 \rho(E) \tag{9.53}$$

where M_{fi} is the matrix element for the transition and $\rho(E)$ is the density of states available at the energy E, or the phase space factor.

In general the matrix element may be unknown; in the extreme case of a constant matrix element the transition rate, and indeed the momentum distributions of the final state particles, are governed by the phase space factor. It is important therefore to be able to compute the latter. In principle, any deviations from phase space provide information about the matrix element.

The state of motion of a single particle, with a momentum whose magnitude is in the range 0–p, confined to a region of space of volume V, can be specified by a 'point' (x, y, z, p_x, p_y, p_z) in the six-dimensional phase space. The limits within which momentum and position can be simultaneously specified are governed by the uncertainty principle with the result that there is an elementary volume or cell in phase space of size h^3 within which states of motion cannot be distinguished. The number N_1 of distinguishable states of motion available to the single particle, then, is given by the total volume of phase space divided by the volume of the elementary cell, i.e.

$$\begin{aligned} N_1 &= \frac{1}{h^3} \int \mathrm{d}x\, \mathrm{d}y\, \mathrm{d}z\, \mathrm{d}p_x\, \mathrm{d}p_y\, \mathrm{d}p_z \\ &= \frac{V}{h^3} \int \mathrm{d}^3 p. \end{aligned} \tag{9.54}$$

For a system of n particles the number of final states N_n is the *product* of the number of final states available to each particle, i.e.

$$N_n = \left(\frac{V}{h^3}\right)^n \int \prod_{i=1}^{n} \mathrm{d}^3 p_i. \tag{9.55}$$

For particles with spin s_i this should be multiplied by $\prod_{i=1}^{n}(2s_i+1)$ but it is convenient to include the spin factor and the constant volume factors in the normalization of the integral and conventionally these are omitted in the definition of the phase space factor. The density of final states $\rho(E)$ is defined as the number of momentum states per unit energy interval, so

$$\rho_n(E) = \frac{\mathrm{d}N_n}{\mathrm{d}E} = \frac{\mathrm{d}}{\mathrm{d}E}\int \prod_{i=1}^{n} \mathrm{d}^3 p_i. \tag{9.56}$$

The integration is performed over all possible values of the individual particle momenta. Because of momentum conservation not all of these are independent but are in fact constrained by the conservation equation

$$\sum_{i=1}^{n} \boldsymbol{p}_i - \boldsymbol{P} = 0 \tag{9.57}$$

where $\boldsymbol{P}$ is the total momentum. This restriction can be accommodated by integrating over all particles except the nth so that the expression for $\rho_n(E)$ becomes

$$\rho_n(E) = \frac{\mathrm{d}}{\mathrm{d}E}\int \prod_{i=1}^{n-1} \mathrm{d}^3 p_i. \tag{9.58}$$

Using the properties of the Dirac δ function (see appendix I and example 9.7) this can be expressed in a more symmetric form with respect to the n particles:

$$\rho_n(E) = \int \prod_{i=1}^{n} \mathrm{d}^3 p_i \delta\left(\sum_{i=1}^{n} \boldsymbol{p}_i - \boldsymbol{P}\right)\delta\left(\sum_{i=1}^{n} E_i - E\right) \tag{9.59}$$

where $\boldsymbol{P}$ is the total momentum and E is the total energy of the n particles. The δ functions embody the constraints imposed on the integral by momentum and energy conservation.

This expression for the density of states factor is not Lorentz invariant while of course the transition rate

$$W = \frac{2\pi}{\hbar}|M_{fi}|^2 \rho_n(E)$$

must be independent of the frame in which it is measured; in this expression the matrix element M_{fi} must therefore also be non-invariant. The following plausibility argument indicates how M_{fi} and $\rho_n(E)$ have to be modified to obtain the relativistically invariant quantities $\mathcal{M}_{fi}$ and $R_n(E)$.

Suppose, for simplicity, a single particle of mass m moves with energy E in a region of space of volume V, and is described by the wavefunction ψ. The usual normalization of the wavefunction, $\int |\psi|^2 \, dV = 1$, implies that the particle density is $1/V$ for an observer at rest with respect to the system. If, on the other hand, the system moves at high speed v with respect to the observer, the volume element will contract along the direction of motion by a factor $\gamma = (1 - v^2/c^2)^{-1/2}$, i.e., in the moving system $dV' = dV/\gamma$, and the particle density apparently increases to γ/V. If, however, the wavefunction is suitably renormalized by the substitution $\psi' \to \sqrt{\gamma}\psi$, then

$$|\mathcal{M}_{fi}|^2 = |M_{fi}|^2 \prod_{j=1}^{n} 2E_j \prod_{i=1}^{n} 2E_i$$

where the index j represents the particles in the initial state and the transition rate is given by

$$W = \frac{2\pi}{\hbar} \frac{|\mathcal{M}_{fi}|^2}{\prod_{j=1}^{n} 2E_j} R_n(E)$$

with

$$R_n(E) = \frac{\rho_n(E)}{\prod_{i=1}^{n} 2E_i}.$$

Thus, explicitly, the Lorentz invariant phase space is given by

$$R_n(E) = \int \prod_{i=1}^{n} \frac{d^3 p_i}{2E_i} \delta\left(\sum_{i=1}^{n} \boldsymbol{p}_i - \boldsymbol{P}\right) \delta\left(\sum_{i=1}^{n} E_i - E\right). \tag{9.60}$$

A calculation of the Lorentz invariant two-body phase space for particles with masses m_1 and m_2 and momenta $\boldsymbol{p}_1$ and $\boldsymbol{p}_2$ in the centre-of-mass system is straightforward (example 9.8). The result is

$$R_2(E) = \frac{\pi p_1}{E} \tag{9.61}$$

where p_1 has the value

$$p_1 = \frac{\{[E^2 - (m_2 - m_1)^2][E^2 - (m_2 + m_1)^2]\}^{1/2}}{2E}. \tag{9.62}$$

Thus, we see that for a given total energy E the two-body phase space factor is just a number. This is also true in general for the n-body phase

space $R_n(E)$ which depends only on the total energy E and the masses of the n particles in the final state. A knowledge of this number is necessary in order to evaluate cross-sections and relative yields (cf. section 8.7.3).

In the general case of three unequal mass particles the Lorentz invariant three-body phase space may be written

$$R_3(E) = \int \frac{4\pi p_3^2 \, \mathrm{d}p_3}{2E_3} \times \frac{\pi\{[E^2 + m_3^2 - 2EE_3 - (m_2 - m_1)^2][E^2 + m_3^2 - 2EE_3 - (m_2 + m_1)^2]\}^{1/2}}{2(E^2 + m_3^2 - 2EE_3)} \tag{9.63}$$

which is an elliptic integral. Frequently, however, what is required is not the value of $R_3(E)$ integrated over all the variables but rather a differential spectrum $\mathrm{d}R_3/\mathrm{d}p_3$ say. In the present case this is

$$\frac{\mathrm{d}R_3}{\mathrm{d}p_3} = \frac{\pi^2 p_3^2}{E_3} \times \frac{\{[E^2 - 2EE_3 + m_3^2 - (m_2 - m_1)^2][E^2 - 2EE_3 + m_3^2 - (m_2 + m_1)^2]\}^{1/2}}{E^2 - 2EE_3 + m_3^2}. \tag{9.64}$$

In a search for resonance production it is more appropriate to use a differential mass spectrum, or invariant mass distribution, than a momentum distribution. The invariant mass distribution $\mathrm{d}R_3/\mathrm{d}M_{12}$ for example may be derived from equation (9.64) using the identity

$$\frac{\mathrm{d}R_3}{\mathrm{d}M_{12}} = \frac{\mathrm{d}R_3}{\mathrm{d}p_3} \frac{\mathrm{d}p_3}{\mathrm{d}M_{12}}$$

with the result

$$\frac{\mathrm{d}R_3}{\mathrm{d}M_{12}} = \frac{\pi^2}{2M_{12}E^2} \times \{[M_{12}^2 - (m_2 - m_1)^2][M_{12}^2 - (m_2 + m_1)^2] \times [E^2 - (M_{12} - m_3)^2][E^2 - (M_{12} + m_3)^2]\}^{1/2} \tag{9.65}$$

(see example 9.9).

In our considerations so far we have dealt only with one-dimensional

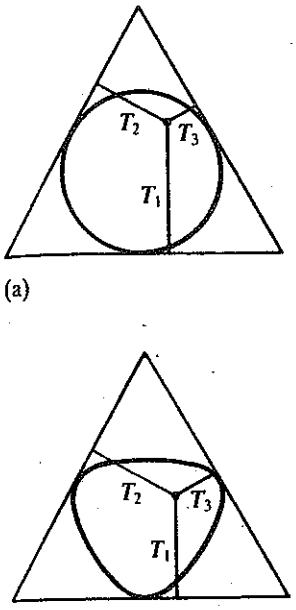

Figure 9.10 Dalitz plot for the three-body decay of a particle. The height of the equilateral triangle is made proportional to the Q value of the decay. Each event is represented by a point whose perpendicular distances from the sides of the triangle are proportional to the kinetic energies T_i of the final state particles. (a) In the non-relativistic case the points are confined to the interior of the inscribed circle and (b) for the relativistic case they are confined to the interior of the inscribed shape.

distributions such as dR/dp and dR/dM. Correlations between different physical variables are often important but these will not be evident in a one-dimensional distribution. For this reason a variety of two-dimensional plots are often used to display experimental results. One of the most widely used is the Dalitz[5] plot, of which various forms exist. A Dalitz plot may be used to study the characteristics of a three-body system produced in a process such as $K^+p \rightarrow K^0p\pi^+$, or the three-body decay of a resonant state such as the classic example of the decay of the ω meson, $\omega \rightarrow \pi^+\pi^-\pi^0$, which we will discuss further in section 9.4. For the latter type of process use is made of the fact that the sum of the perpendicular distances from the sides of an equilateral triangle to a point inside the triangle is equal to the height of the triangle. The Q value of the decay is given by

$$Q = m_\omega - 3m_\pi = \sum_{i=1}^{3} T_i$$

where m_ω and m_π are the masses of the ω and π respectively and T_i is the kinetic energy of the ith pion in the ω rest system. Thus, if the height of the triangle is made equal to Q, each decay can be represented by a point with the perpendicular distances to the sides of the triangle given by T_i, as shown in figure 9.10. For three equal mass particles moving with non-relativistic velocities, conservation of energy and momentum restricts the points to the interior of the inscribed circle, figure 9.10(a). In the relativistic case, which has been treated by Fabri,[6] the points are restricted to the interior of the inscribed shape shown in figure 9.10(b), which in the ultra-relativistic case becomes a triangle.

A different type of Dalitz plot is used to study a three-body final state produced in a scattering process. If we label the final state particles 1, 2 and 3 then the kinetic energies of any two particles, say 1 and 2, are chosen to specify the final state and the Dalitz plot is a plot of T_1 against T_2 as shown in figure 9.11(a).

The kinetic energy of particle 1 is linearly related to the square of the

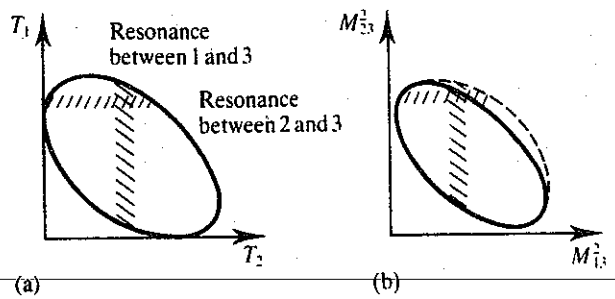

Figure 9.11 Schematic diagrams of Dalitz plots for three-body final states showing resonance formation between pairs of particles. In part (a) the position of a resonance varies as the total energy available varies. In part (b) the boundary of the plot varies but the position of a resonance remains fixed.

effective mass of particles 2 and 3 through the relation

$$T_1 = \frac{(E - m_1)^2 - M_{23}^2}{2E} \tag{9.66}$$

where E is the total energy in the centre-of-mass system, m_1 is the mass of particle 1 and M_{23} is the invariant mass of particles 2 and 3. A more widely used form of Dalitz plot is one in which the square of the invariant mass of one pair of particles is plotted against the invariant mass squared of another pair, as shown in figure 9.11(b).

Each type of Dalitz plot described above has the important property that equal areas in the plot correspond to equal volumes in the Lorentz invariant three-body phase space R_3, i.e.

$$\mathrm{d}R_3 \propto \mathrm{d}T_1\, \mathrm{d}T_2 \propto \mathrm{d}M_{23}^2\, \mathrm{d}M_{13}^2. \tag{9.67}$$

In the absence of final state interactions the density of points in the Dalitz plot will therefore be uniform. In general, the density of points is proportional to the square of the invariant matrix element for the reaction. If a resonance occurs between particles 2 and 3 say, there will be an increased density of points in a band at fixed T_1 in the Dalitz plot in figure 9.11(a), or fixed M_{23}^2 in figure 9.11(b). The boundary of the Dalitz plot is fixed by momentum conservation and the total energy available to the system. The disadvantage of the type of Dalitz plot shown in figure 9.11(a) is that the position of a resonance on the plot varies with the total energy available, thus making it difficult to combine the results of experiments performed at different energies if the data are presented in this form. A plot of the squared effective masses overcomes this difficulty; an increase in the total energy simply changes the contour of the plot but does not alter the position of a resonance. This is shown schematically in figure 9.11(b).

We end this section with a proof of (9.67). As we saw earlier, the Lorentz invariant three-body phase space is given by

$$R_3 = \int \frac{\mathrm{d}^3p_1\, \mathrm{d}^3p_2\, \mathrm{d}^3p_3}{8E_1E_2E_3}\, \delta(\boldsymbol{p}_1 + \boldsymbol{p}_2 + \boldsymbol{p}_3)\delta(E_1 + E_2 + E_3 - E)$$

which, when integrated over $\boldsymbol{p}_3$, gives

$$R_3 = \int \frac{1}{8E_1E_2E_3}\, p_1^2\, \mathrm{d}p_1\, \mathrm{d}\Omega_1\, p_2^2\, \mathrm{d}p_2\, \mathrm{d}\Omega_2 \delta(E_1 + E_2 + E_3 - E)$$

where $\mathrm{d}\Omega_1 = \mathrm{d}(\cos\theta_1)\, \mathrm{d}\phi_1$ and $\mathrm{d}\Omega_2 = \mathrm{d}(\cos\theta_2)\, \mathrm{d}\phi_2$, θ_i and ϕ_i being the spherical polar angles specifying the directions of particles 1 and 2. Instead of the polar angle θ_2 it is convenient to introduce the angle θ_{12}, the angle

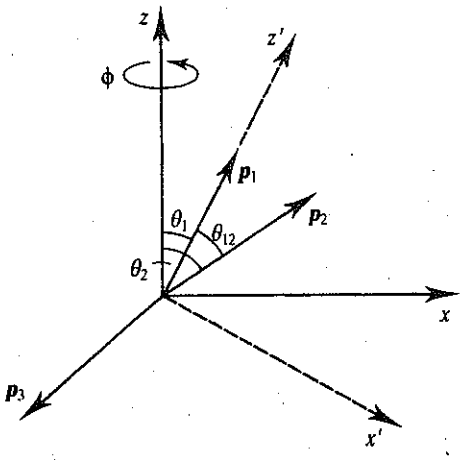

Figure 9.12
Definition of the angles used in the integration of R_3. p_1, p_2 and p_3 are the momenta of the three particles in the centre-of-mass system.

between $\boldsymbol{p}_1$ and $\boldsymbol{p}_2$ as shown in figure 9.12. The conservation of momentum restricts the three momenta $\boldsymbol{p}_1$, $\boldsymbol{p}_2$ and $\boldsymbol{p}_3$ to lie in a plane, which without loss of generality we choose to be the z–x plane. For a given orientation of $\boldsymbol{p}_1$ we can choose the z axis to be along $\boldsymbol{p}_1$ and then

$$\int \mathrm{d}\Omega_2 = \int \mathrm{d}(\cos\theta_2)\,\mathrm{d}\phi_2 = \int \mathrm{d}(\cos\theta_{12})\,\mathrm{d}\phi_2.$$

Then

$$R_3 = \int \frac{1}{8E_1E_2E_3}\, p_1^2\,\mathrm{d}p_1\,\mathrm{d}\Omega_1 p_2^2\,\mathrm{d}p_2\,\mathrm{d}(\cos\theta_{12})\,\mathrm{d}\phi_2\delta(E_1+E_2+E_3-E)$$

which, when integrated over all space angles except θ_{12}, becomes

$$R_3 = \int \frac{\pi^2}{E_1E_2E_3}\, p_1^2\,\mathrm{d}p_1 p_2^2\,\mathrm{d}p_2\,\mathrm{d}(\cos\theta_{12})\delta(E_1+E_2+E_3-E).$$

For fixed $\boldsymbol{p}_1$ and $\boldsymbol{p}_2$ the angle between $\boldsymbol{p}_1$ and $\boldsymbol{p}_2$ is given by momentum conservation by the relation

$$p_3^2 = p_1^2 + p_2^2 + 2p_1p_2\cos\theta_{12}$$

from which it follows that

$$p_3\,\mathrm{d}p_3 = p_1p_2\,\mathrm{d}(\cos\theta_{12}).$$

On substitution for $\mathrm{d}(\cos\theta_{12})$ the expression for R_3 becomes

$$R_3 = \pi^2 \int \frac{p_1\,dp_1p_2\,\mathrm{d}p_2p_3\,\mathrm{d}p_3}{E_1E_2E_3}\,\delta(E_1+E_2+E_3-E).$$

Since, for an individual particle, $p^2 = E^2 - m^2$, we have $p\,\mathrm{d}p = E\,\mathrm{d}E = E\,\mathrm{d}T$, so that

$$R_3 = \pi^2 \int \mathrm{d}T_1\,\mathrm{d}T_2\,\mathrm{d}T_3\,\delta(E_1 + E_2 + E_3 - E).$$

Integration over T_3 gives the required result,

$$\mathrm{d}R_3 \propto \mathrm{d}T_1\,\mathrm{d}T_2.$$

Finally, equation (9.66) yields, on differentiation

$$\mathrm{d}T_1 \propto \mathrm{d}M_{23}^2$$

and similarly

$$\mathrm{d}T_2 \propto \mathrm{d}M_{13}^2$$

and therefore

$$\mathrm{d}R_3 \propto \mathrm{d}M_{23}^2\,\mathrm{d}M_{13}^2.$$

9.4 *Production experiments*

Many years of experimentation have shown that there are precisely nine mesons with spin-parity 0^-. The well-known π and K mesons, together with the I spin singlet η and $\eta'(958)$ states, form a nonet of pseudoscalar mesons. In SU(3) these nine states are further subdivided into an octet and singlet (section 10.3). Meson states with higher spins, $J^P = 1^-, 2^+$ for example, repeat this multiplet structure. In the baryon sector the octet of $\frac{1}{2}^+$ stable baryons is accompanied by a decuplet of $\frac{3}{2}^+$ baryons, the I spin quartet of $\Delta(1232)$ resonances, the $\Sigma(1385)$ triplet, the $\Xi(1530)$ doublet and the Ω^-. The quark model (chapter 10) successfully accounts for the observed multiplet structure in the hadron spectrum. In the present section we describe some of the techniques used in the analysis of production experiments to determine the quantum numbers of resonant states.

The η meson

The η was first observed[7] in an exposure of the Lawrence Radiation Laboratory 72 inch deuterium-filled bubble chamber to a beam of 1.23 GeV/c π^+ mesons. The three-pion invariant mass distribution (figure 9.13(a)) for the reaction $\pi^+\mathrm{d} \rightarrow \mathrm{pp}\pi^+\pi^-\pi^0$ clearly shows η and ω meson production. The Dalitz plot for a compilation[8] of decays $\eta \rightarrow \pi^+\pi^-\pi^0$

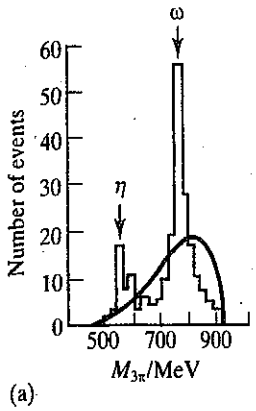

(a)

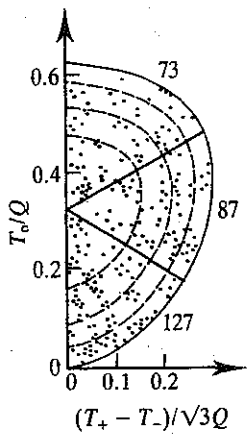

(b)

Figure 9.13
(a) Invariant mass distribution of the three-pion system in the reaction $\pi^+ d \rightarrow pp\pi^+\pi^-\pi^0$. The solid curve is the phase space prediction. (After Pevsner A *et al.* 1961 *Phys Rev Lett* 7 (421).) (b) Dalitz plot for the decay $\eta \rightarrow \pi^+\pi^-\pi^0$. Normalized Dalitz plot variables T_0/Q and $(T_+ - T_-)/\sqrt{3}Q$, where T_0, T_+ and T_- are the kinetic energies of the π^0, π^+ and π^- respectively, have been used. The plot has been folded about the T_0/Q axis. (After Alff C *et al.* 1962 *Phys Rev Lett* **9** (325).)

(figure 9.13(b)) has a distribution of events which is compatible only with the spin-parity assignment 0^- for the η meson.

In addition to the decay mode $\eta \rightarrow \pi^+\pi^-\pi^0$, several others have been seen, the most dominant of which, together with the branching fractions, are

$$\eta \rightarrow \begin{cases} \pi^+\pi^-\pi^0 & 23.6 \pm 0.6 \text{ per cent} \\ \pi^0\pi^0\pi^0 & 31.9 \pm 0.4 \text{ per cent} \\ \gamma\gamma & 38.9 \pm 0.5 \text{ per cent} \\ \pi^+\pi^-\gamma & 4.88 \pm 0.15 \text{ per cent} \end{cases}$$

The decay $\eta \rightarrow 2\gamma$ is clearly electromagnetic and because the branching fractions of the other decay modes are comparable with that for $\eta \rightarrow 2\gamma$, these too can be assumed to be electromagnetic. This assumption is consistent with the measured width $\Gamma_\eta = 1.19 \pm 0.11$ keV, which corresponds to a lifetime of roughly 10^{-18} s and is supported below by an argument based on *G*-parity. Since electromagnetic decays are invariant under charge conjugation and the *C*-parity of the photon is -1, the η has *C*-parity $+1$ so that, like the π^0, the η^0 and its antiparticle are indistinguishable.

Historically, the decay $\eta \rightarrow \pi^+\pi^-\pi^0$ has in fact proved to be important in testing *C* invariance in electromagnetic interactions. If the decay is invariant under charge conjugation there should be no asymmetry between the π^+ and π^- in the η decays, i.e. the Dalitz plot should be symmetric about the vertical axis. (In figure 9.13(b) the Dalitz plot has been folded about this axis, on the assumption that the decay is *C* invariant.) It is usual to define the asymmetry as

$$A = \frac{N_+ - N_-}{N_+ + N_-}$$

where N_+ is the number of events in which the π^+ has greater energy than the π^- in the η rest system and N_- is the number of events in which the π^- has the greater energy. Charge conjugation invariance implies that A should be zero. In an analysis of over 220 000 events Layter *et al.*[9] obtained the value $A = -0.0005 \pm 0.0022$ and thus found no evidence for *C*-violating effects.

We recall (section 8.11) that both *C* and *G* (charge conjugation followed by a rotation of π about the 2 axis in *I* spin space) are conserved quantities in the strong interactions. Since *C* is conserved in both strong and electromagnetic interactions it follows that if *G* is violated in a process that is not weak then *I* spin is not conserved or, in other words, the process takes place via the electromagnetic interaction. The η meson has no charged partners and therefore it follows that the *G*-parity of the η is also $+1$. The *G*-parity of a system of n pions is $(-1)^n$ and thus the decay

$\eta \rightarrow \pi^+\pi^-\pi^0$ violates G-parity and is therefore electromagnetic. This conclusion can equally well be reached by the observation that the decay $\eta \rightarrow \pi^0\pi^0\pi^0$ does not conserve I spin; the I spin of a three-pi-zero system is necessarily greater than or equal to 1.

In summary, the quantum numbers $I^G J^{PC}$ of the η meson are 0^+0^{-+}.

The $\rho(770)$

The ρ meson has a mass and width of 768.1 ± 0.5 MeV and 151.5 ± 1.2 MeV respectively and decays to two pions with a branching fraction of essentially 100 per cent. It exists in three charge states ρ^+, ρ^- and ρ^0 and therefore has $I = 1$.

The very large width and hence very short lifetime of the ρ meson means that the decay $\rho \rightarrow \pi\pi$ is a strong interaction. The conservation of G-parity therefore implies that $G(\rho) = +1$. Since $G = \exp(i\pi I_2)C$, it follows that $C(\rho) = -1$. Furthermore, the charge conjugation operation C on a $\pi^+\pi^-$ system is equivalent to a spatial inversion, and therefore $C = (-1)^l$, where l is the relative orbital angular momentum between the π^+ and π^-; l must therefore be odd. Conservation of angular momentum and parity in the decay $\rho \rightarrow \pi\pi$ therefore implies that the ρ meson must have a spin-parity in the series $1^-, 3^- \ldots$. Which of these possibilities is the correct one may be determined by analysing the angular distribution of the pions in the dipion rest frame as outlined below.

The dominant mechanism for ρ production in the reaction $\pi^-p \rightarrow p\pi^-\pi^0$, for example, is single pion exchange as shown in figure 9.14(a), so that ρ production can be viewed as the result of scattering of the incident π^- and the exchanged pion π^0_{ex}. This scattering process is conventionally analysed in the ρ rest frame (figure 9.14(b)) in which the z axis is chosen as the direction of the incident pion and the y axis is defined as the normal to the scattering plane

$$y = \frac{\boldsymbol{p}_{in} \wedge \boldsymbol{p}_{out}}{|\boldsymbol{p}_{in} \wedge \boldsymbol{p}_{out}|}$$

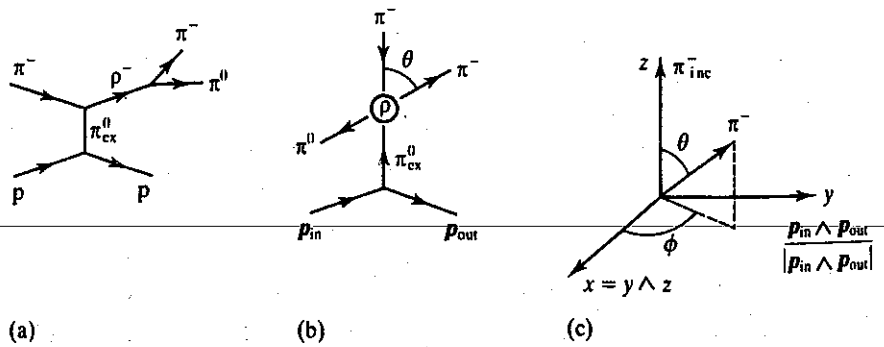

Figure 9.14
Production and decay of the ρ meson: (a) the pion exchange graph; (b) the configuration in the ρ rest system; (c) the Gottfried–Jackson coordinate system.

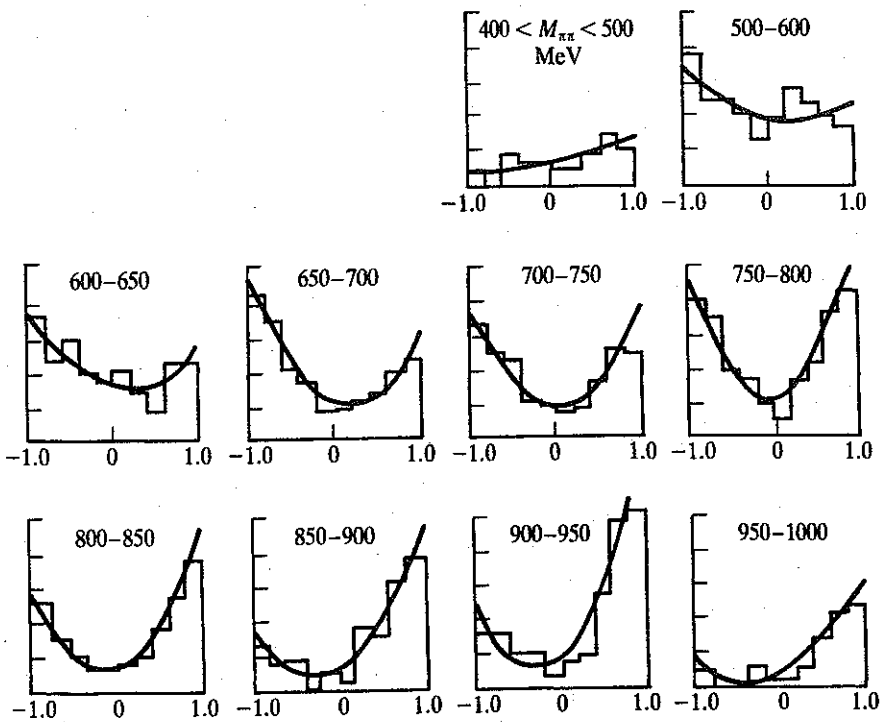

Figure 9.15 The $\pi^-\pi^0$ angular distribution in the dipion rest system, for the reaction $\pi^-p \to p\pi^-\pi^0$, as a function of $\pi^-\pi^0$ invariant mass. (After Walker W D *et al.* 1967 *Phys Rev Lett* **18** (630).)

where $\boldsymbol{p}_{\text{in}}$ and $\boldsymbol{p}_{\text{out}}$ are the momenta of the proton in the inital and final states respectively. The x axis is given by $\boldsymbol{x} = \boldsymbol{y} \wedge \boldsymbol{z}$ (figure 9.14(c)). This frame of reference is known as the Gottfried–Jackson frame. The partial wave formalism developed in section 9.2.1 for the scattering of spinless particles is applicable here. Figure 9.15 shows the distributions in $\cos\theta$, where θ is the π–π scattering angle in the dipion rest system, as a function of the dipion effective mass (total energy in the dipion rest system), obtained by Walker *et al.*[10] These angular distributions are adequately described by an expression of the form

$$I(\theta) = A_0 + A_1 \cos\theta + A_2 \cos^2\theta. \tag{9.68}$$

As expected for the scattering of spinless particles the distributions are isotropic in the azimuthal angle ϕ. The partial wave expansion equation (9.16), using S and P waves only, gives

$$\begin{aligned} I(\theta) &= \frac{1}{k^2}|T_0 + 3T_1\cos\theta|^2 \\ &= \frac{1}{k^2}(|T_0|^2 + 6\,\text{Re}\,T_0T_1^*\cos\theta + 9|T_1|^2\cos^2\theta) \end{aligned} \tag{9.69}$$

which has the same form as equation (9.68). Here T_l is the amplitude for the lth partial wave.

Since pions are bosons the overall wavefunction of the π^-–π^0 system

$$\Psi = \psi(\text{space})I(I \text{ spin})$$

must be symmetric with respect to exchange of the two pions. A $\pi^-\pi^0$ system can have either $I = 1$ or $I = 2$ and, using the table of Clebsch–Gordan coefficients for the coupling of two $I = 1$ particles, the $I = 1$ state is

$$|1, -1\rangle = \frac{1}{\sqrt{2}}(|\pi^0\rangle|\pi^-\rangle - |\pi^-\rangle|\pi^0\rangle)$$

which is antisymmetric, and the $I = 2$ state is

$$|2, -1\rangle = \frac{1}{\sqrt{2}}(|\pi^0\rangle|\pi^-\rangle + |\pi^-\rangle|\pi^0\rangle)$$

which is symmetric. The symmetry requirement therefore means that P wave scattering takes place in the $I = 1$ state and S wave scattering in the $I = 2$ state. The ρ meson, with $I = 1$, is therefore a P wave π–π resonance with $J^P = 1^-$. If the S wave amplitude is predominantly real, the asymmetry term will vanish at the resonance mass, where T_1 becomes purely imaginary, and should change sign on passing through the resonant energy. This is borne out by the experimental results in figure 9.15. In conclusion, the ρ meson has $I = 1$, $G = 1$, $C = -1$ and $J^P = 1^-$.

The $\omega(783)$

The ω meson was first observed by Maglic *et al.*[11] in a bubble chamber study of the annihilation process

$$\bar{p} + p \rightarrow \pi^+ + \pi^+ + \pi^- + \pi^- + \pi^0.$$

Figure 9.16 shows the three-pion effective mass distributions for various charge states. The neutral combinations $\pi^+\pi^-\pi^0$ show a narrow resonance centred at a mass of 787 MeV/c^2, which is absent in all other charge combinations with $|Q| \geqslant 1$. The ω meson therefore has I spin 0. The decay $\omega \rightarrow \pi^+\pi^-\pi^0$ proceeds via the strong interaction and therefore the ω has G-parity $(-1)^3 = -1$.

Because the determination of the spin-parity of the ω meson is a classic of its kind we describe in some detail how the analysis[12] of the distribution of events in the decay Dalitz plot led to the assignment $J^P = 1^-$.

We first note that since the I spin of the ω is $I_\omega = 0$ its isospin wavefunction Φ_ω must be a scalar. The only way to construct an isoscalar

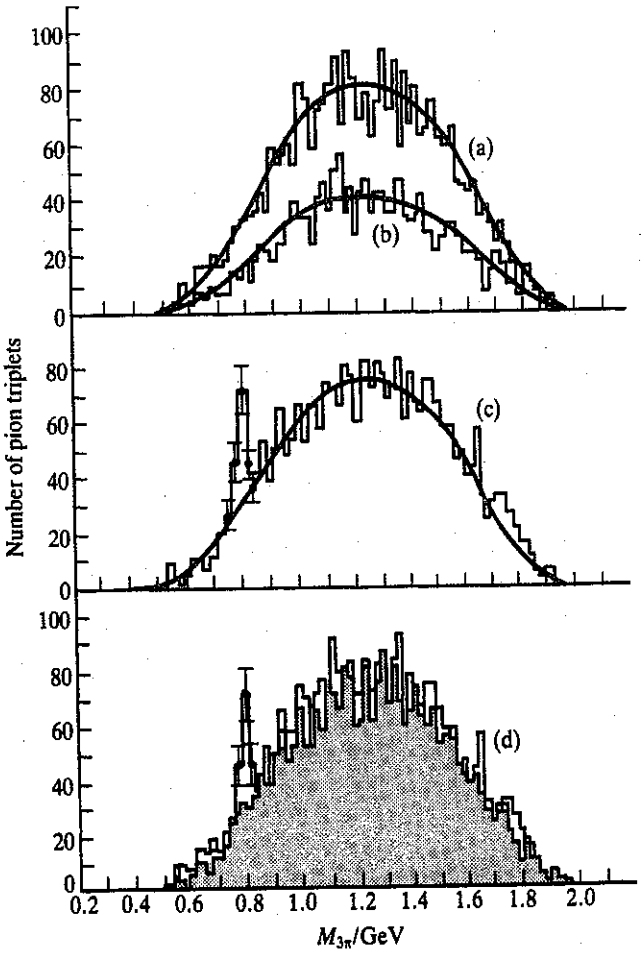

Figure 9.16 Three-pion invariant mass distributions from the annihilation process $\bar{p}p \rightarrow \pi^+\pi^+\pi^-\pi^-\pi^0$: curve (a), $\pi^+\pi^+\pi^-$ and $\pi^+\pi^-\pi^-$ combinations; curve (b), $\pi^+\pi^+\pi^0$ and $\pi^-\pi^-\pi^0$ combinations; curve (c), $\pi^+\pi^-\pi^0$ combinations. In (d) the combinations (a) and (b) (shaded) are contrasted with (c). The ω meson appears only in the neutral charge state $\pi^+\pi^-\pi^0$. (After Maglic B C *et al.* 1961 *Phys Rev Lett* 7 (178).)

from the isovector wavefunctions $\boldsymbol{\Phi}_1$, $\boldsymbol{\Phi}_2$ and $\boldsymbol{\Phi}_3$ of the three pions is to form a triple product:

$$\Phi_\omega = \Phi_1 \cdot (\Phi_2 \wedge \Phi_3) = \Phi_2 \cdot (\Phi_3 \wedge \Phi_1) = \Phi_3 \cdot (\Phi_1 \wedge \Phi_2). \qquad (9.70)$$

These triple products are antisymmetric with respect to interchange of any two pions. The total wavefunction for three bosons

$$\Psi_{\text{tot}} = \Phi(I \text{ spin})\, \psi(\text{space})$$

is required by Bose–Einstein statistics to be symmetric under interchange of any two particles and therefore the spatial wavefunction must be antisymmetric. This will influence the distribution of events in the Dalitz

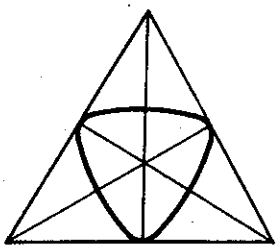

Figure 9.17
The ω decay Dalitz plot showing the symmetry axes.

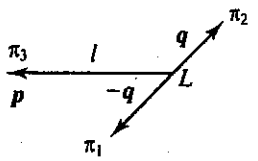

(a)

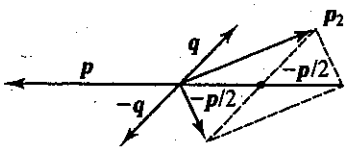

(b)

Figure 9.18
Definition of the variables used in the analysis of ω decay. (a) In the dipion system π_1 and π_2 have momenta $-\boldsymbol{q}$ and $\boldsymbol{q}$ respectively and the relative orbital angular momentum is L. The third pion π_3 has momentum $\boldsymbol{p}$ and orbital angular momentum $\boldsymbol{l}$ with respect to the dipions in the three-pion rest system. (b) Non-relativistic transformation to the overall three-pion rest system

plot. The type of Dalitz plot used is the conventional one for studying the three-body decay of a resonance (figure 9.17). Since the spatial wavefunction is totally antisymmetric the matrix element squared must be symmetric under the interchange of any pair of pions and therefore the density of points must be invariant under a reflection through any of the symmetry axes of the Dalitz plot shown in figure 9.17. This observation is borne out by the experimental results and means that the Dalitz plot can be folded about these axes thereby concentrating all the events in one sextant. The statistical accuracy of the analysis is thereby increased.

We turn now to an evaluation of the general forms of the matrix element $M(p_i, E_i)$, in terms of the momenta and energies of the three pions, for different values of the ω spin-parity. In this context we note that a scalar meson with $J^P = 0^+$ cannot decay via a parity-conserving strong interaction to three pseudoscalar mesons. We consider three possible spin-parity assignments for the ω, namely pseudoscalar 0^-, vector 1^- and axial vector 1^+. We will construct the matrix elements initially in terms of the variables shown in figure 9.18(a) in which we envisage a dipion system π_1 and π_2 with a relative orbital angular momentum L in the dipion rest frame and a single pion π_3. The single pion and the dipion system are assumed to have a relative angular momentum l in the overall three-pion rest system. The momentum $\boldsymbol{q}$ is the momentum in the dipion rest system and $\boldsymbol{p}$ is the momentum of π_3 in the three-pion rest system. In the non-relativistic limit the spin J of the ω meson is $\boldsymbol{J} = \boldsymbol{l} + \boldsymbol{L}$.

Pseudoscalar ω, $J^P = 0^-$

Since the intrinsic parity of the three pions is $(-1)^3 = -1$ the matrix element for the decay of a pseudoscalar meson must have the properties of a scalar. Bearing in mind that we must construct a matrix element which is antisymmetric with respect to interchange of any two pions we write

$$M(0^-) \approx \boldsymbol{p}\cdot\boldsymbol{q}.$$

This matrix element is odd under the interchange of π_1 and π_2 for then $\boldsymbol{q} \to -\boldsymbol{q}$. Our aim is to recast this in a form which is symmetric in the labels of all three pions and which is written in terms of variables in the three-pion rest system. With reference to figure 9.18(b) and using the non-relativistic expression for the kinetic energy, the total energies of π_1 and π_2 are

$$E_1 = \frac{1}{2m}\left(-\frac{\boldsymbol{p}}{2} - \boldsymbol{q}\right)^2 + m$$

$$E_2 = \frac{1}{2m}\left(-\frac{\boldsymbol{p}}{2} + \boldsymbol{q}\right)^2 + m$$

from which it follows that

$$M(E_1 - E_2) = \boldsymbol{p}\cdot\boldsymbol{q}.$$

The matrix element for the decay of a 0^- ω is then of the form

$$M(0^-) \approx (E_1 - E_2)(E_2 - E_3)(E_3 - E_1)$$

This matrix element, and hence the density of points in the Dalitz plot, will vanish whenever two of the pions have equal energies, i.e. along the symmetry lines and in particular at the centre of the Dalitz plot where all three pions have the same energy (figure 9.19).

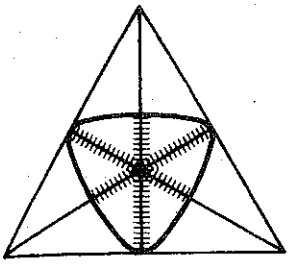

Figure 9.19
Schematic diagram showing where the density of points will vanish for a $J^P = 0^-$ ω meson.

Vector ω, $J^P = 1^-$
In this case, taking into account the negative intrinsic parity of the three-pion system, the matrix element must have the properties of an axial vector, i.e. one that does not change sign under a parity transformation. The simplest possibility for the orbital angular momenta are $L = l = 1$ and the matrix element will be of the form

$$M(1^-) \approx \boldsymbol{p} \wedge \boldsymbol{q}.$$

Using the fact that $\boldsymbol{p}_3 \equiv \boldsymbol{p}$, $\boldsymbol{p}_1 = -(\boldsymbol{p}/2) + \boldsymbol{q}$, $\boldsymbol{p}_2 = -(\boldsymbol{p}/2) - \boldsymbol{q}$ and symmetrizing with respect to the labels of the three pions we have

$$M(1^-) \approx \boldsymbol{p}_1 \wedge \boldsymbol{p}_2 + \boldsymbol{p}_2 \wedge \boldsymbol{p}_3 + \boldsymbol{p}_3 \wedge \boldsymbol{p}_1.$$

In marked contrast to the case above for a pseudoscalar ω, the matrix element in this case vanishes whenever the pions are collinear. The density of points should therefore approach zero around the boundary of the Dalitz plot as shown schematically in figure 9.20.

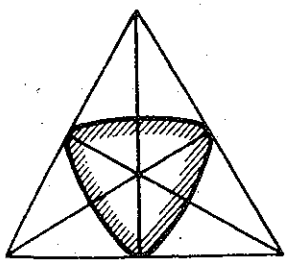

Figure 9.20
The density of points in the Dalitz plot vanishes around the boundary if the ω has $J^P = 1^-$.

Axial vector ω, $J^P = 1^+$
The matrix element in this case must have the properties of an ordinary or polar vector. The simplest configuration is that in which $l = 0$ and $L = 1$ and the matrix element can be written in the form

$$M(1^+) \approx E_3\boldsymbol{q}.$$

Since $\boldsymbol{q} = \frac{1}{2}(\boldsymbol{p}_1 - \boldsymbol{p}_2)$ the matrix element, when symmetrized with respect to the labels of the three pions, becomes

$$M(1^+) \approx E_3(\boldsymbol{p}_1 - \boldsymbol{p}_2) + E_2(\boldsymbol{p}_3 - \boldsymbol{p}_1) + E_1(\boldsymbol{p}_2 - \boldsymbol{p}_3).$$

This matrix element vanishes whenever $E_1 = E_2 = E_3$, i.e. at the centre

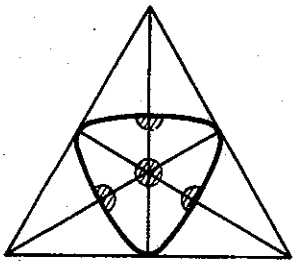

Figure 9.21
Regions of vanishing density for $J^P = 1^+$.

of the Dalitz plot, and whenever two pions have the same momenta which occurs in the regions shown in figure 9.21. The above general arguments display only the gross features of the variation of the density of points on the Dalitz plot. The detailed variation for different spin-parities is illustrated in the isometric drawings of figures 9.22(a)–9.22(c) for 0^-, 1^- and 1^+ mesons respectively. Because the resonance has a finite width, the Q value of the decay, and hence the boundary of the Dalitz plot, varies from event to event. For this reason, normalized variables T_i/Q are used as Dalitz plot variables. The height above the plane is proportional to the matrix element squared, $|M|^2$, and the maximum height above the plane is chosen as 1. Contours of equal $|M|^2$ are shown at 0.2 intervals. For a comparison of these $|M|^2$ distributions with the experimental results, both the results and $|M|^2$ have been folded about the symmetry lines of the Dalitz plot.

Figure 9.23(a) shows this folded Dalitz plot for events in the ω peak. The

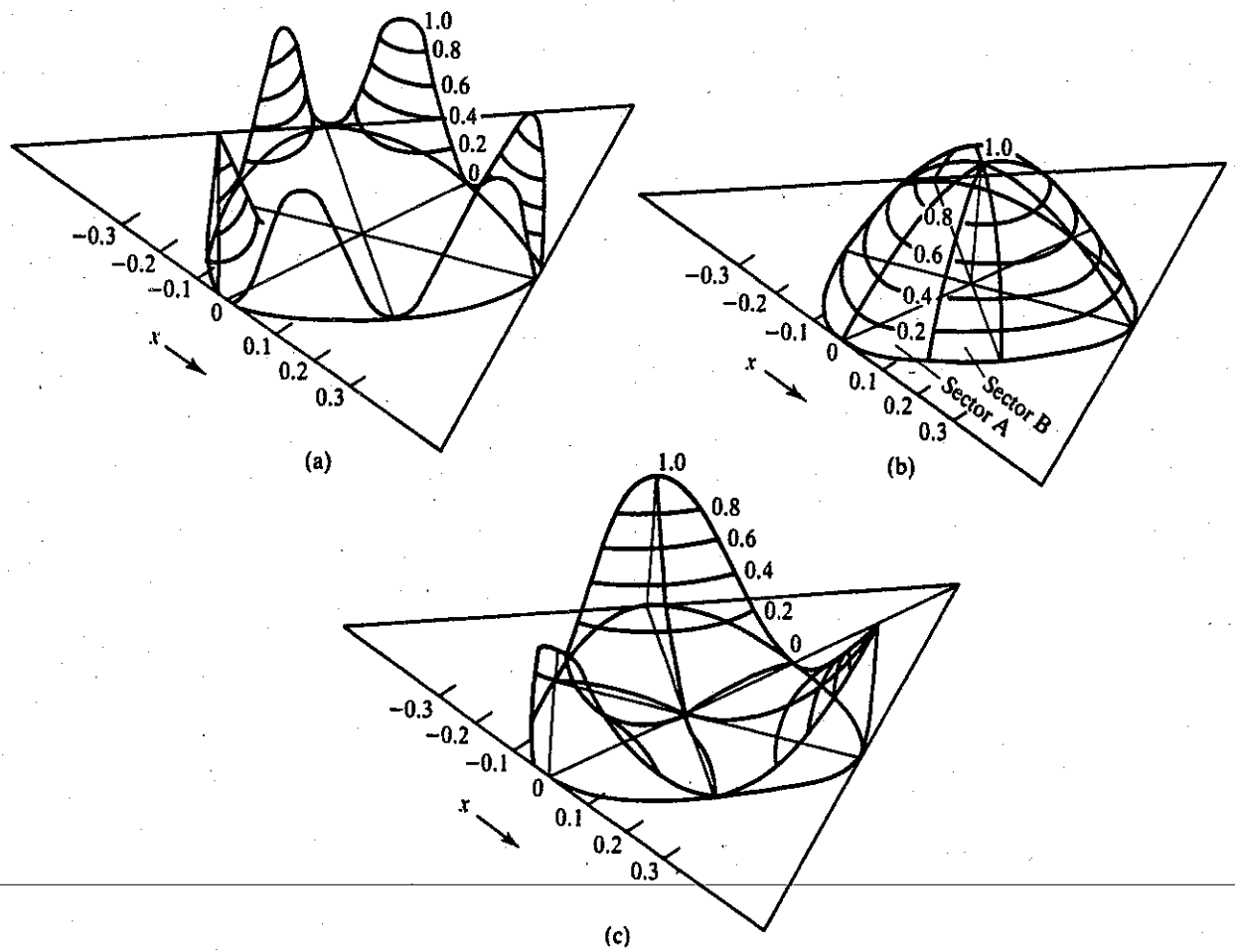

Figure 9.22 Isometric drawings showing the detailed density distributions in the Dalitz plot for (a) a 0^-, (b) a 1^- and (c) a 1^+ ω meson.

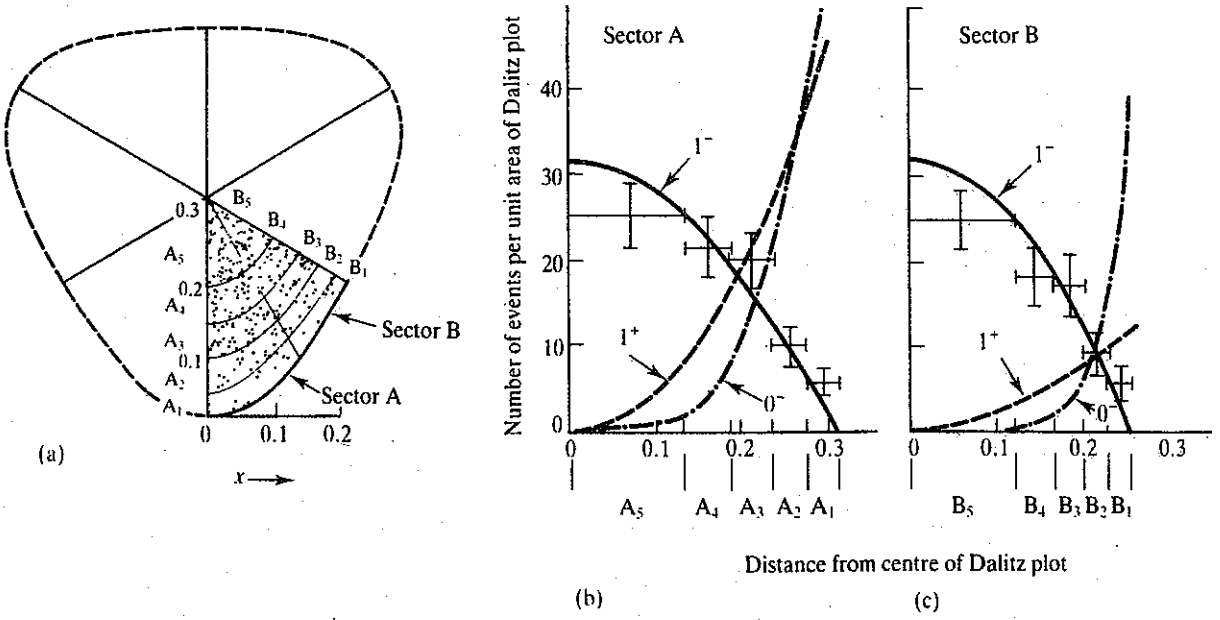

Figure 9.23 (a) Distribution of events in the folded Dalitz plot for events in the ω peak; (b), (c) distribution of events in the subsectors A_i and B_i with the theoretical expectations for $J^P = 0^-$, 1^- and 1^+. (After Stevenson M L *et al.* 1962 *Phys Rev* **125** (687).)

contours on the figure are formed by projecting the contours of the isometric drawing, for the case of a 1^- meson, onto the plane of the Dalitz plot. Since the matrix elements show considerable 'azimuthal' variation, the folded area was arbitrarily divided into two sectors A and B. The contours in turn divide each sector into five subsectors $A_1, \ldots, A_5$, $B_1, \ldots, B_5$. The number of events per unit area within $A_1, \ldots, A_5$, $B_1, \ldots, B_5$ are shown in figures 9.23(b) and 9.23(c). The curves are the predictions for the three J^P values considered and it is clear from the comparison with the data that the ω meson has $J^P = 1^-$.

REFERENCES 9

1 **Watson G N** 1944 *Theory of Bessel Functions* Macmillan

2 **Blatt J M and Weisskopf V F** 1952 *Theoretical Nuclear Physics* Wiley

3 **Bussey P J** *et al.* 1973 *Nucl Phys* **B58** (363)

4 **Particle Data Group** 1992 'Review of particle properties' *Phys Rev* **D45**

5 **Dalitz R H** 1953 *Phil Mag* **44** (1068)

6 **Fabri E** 1954 *Nuovo Cimento* **11** (479)

7 **Pevsner A** *et al.* 1961 *Phys Rev Lett* **7** (421)

8 **Alff C** *et al.* 1962 *Phys Rev Lett* **9** (325)

9 **Layter J G** *et al.* 1972 *Phys Rev Lett* **29** (316)